

THESEUS WORKSHOP
NAPOLI, 5-6 OCT. 2017

X-RAY FLARE IN GRB

Yu Wang

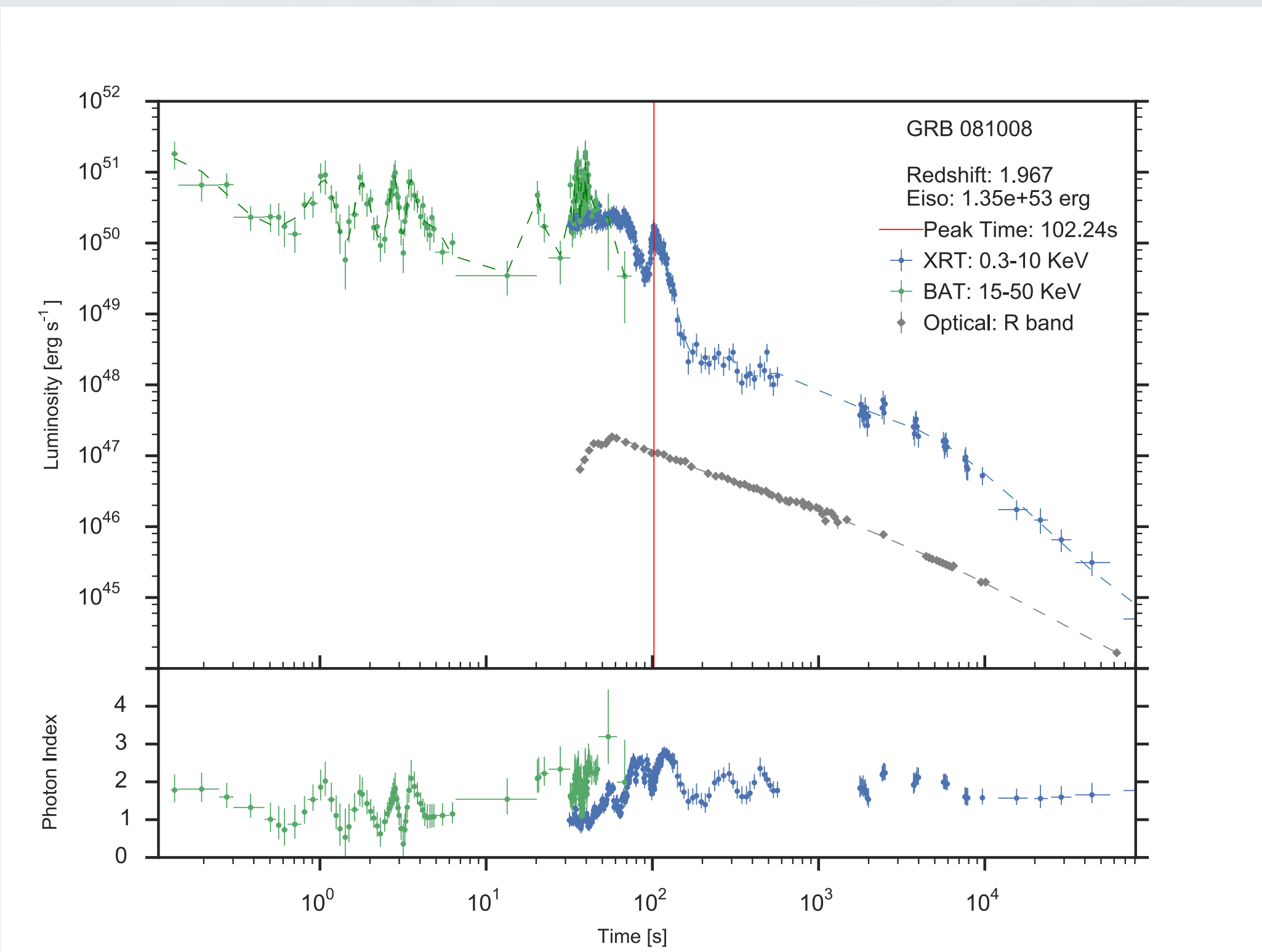
COLLABORATION: R. RUFFINI, Y. AIMURATOV, L. BECERRA,
C. L. BIANCO, M. KARLICA, M. KOVACEVIC, L. LI, J. D. MELON FUKSMAN,
R. MORADI, M. MUCCINO, A. V. PENACCHIONI, G. B. PISANI,
D. PRIMORAC, J. A. RUEDA, S. SHAKERI, G. V. VERESHCHAGIN, AND S.-S. XUE

AFFILIATION: ICRANET & SAPIENZA UNIVERSITY

INDEX

- Sample selection
- Statistical Correlations between Eiso and flares features
- Thermal emission in the flares
- Model and Simulation

LUMINOSITY LIGHT-CURVE & X-RAY FLARE



QUESTION

Mechanism of X-ray flare ?

- Are all the X-ray flares from the same mechanism?
- Are X-ray flares and prompt spikes from the same mechanism ?

X-RAY FLARES

SAMPLE
SELECTION

OBSERVATIONS & STATISTICS

Previous statistical papers

To collect as more flares as possible

All X-ray flares
in all GRBs

Including GRBs without
Known redshift

Ignoring possible findings and
correlations existing in specific
classes of GRBs.

Using observed value.
Inappropriate to analyze the
physical origins, especially for
high redshift GRBs.

OBSERVATIONS & STATISTICS

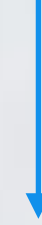
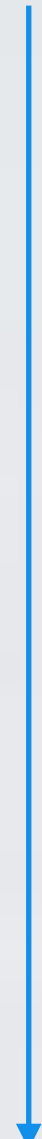
Our Approach

To find a sample of flares possibly from a same mechanism

Hypothesis

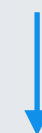
Including GRBs only with
Known redshift

All the quantities are corrected
and transferred to the
cosmological rest frame

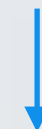


HYPOTHESIS

Flares with distinct observed patterns could be produced by various mechanisms



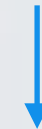
select flares sharing similar morphologies



CRITERIA

- 1) Flares in the long GRBs
- 2) Flares occurring before the plateau phase (early time flare)

X-ray flares could have different mechanisms from the prompt spikes



CRITERIA

- 3) Exclude flares that other bands dominate soft X-ray band
- 4) Exclude flares contaminated by the prompt emission

CLEAR FLARE FOR DATA ANALYSIS

CRITERIA

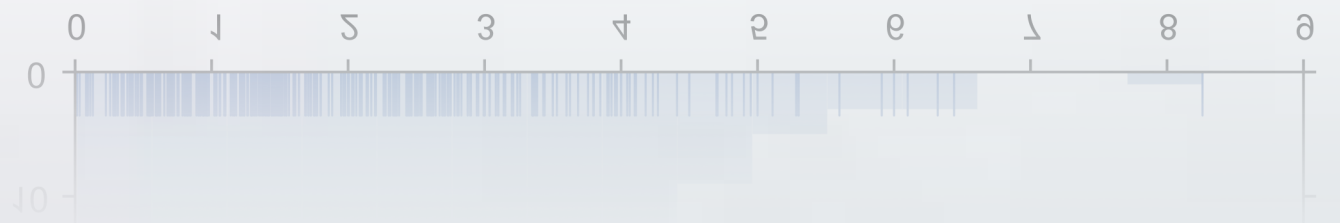
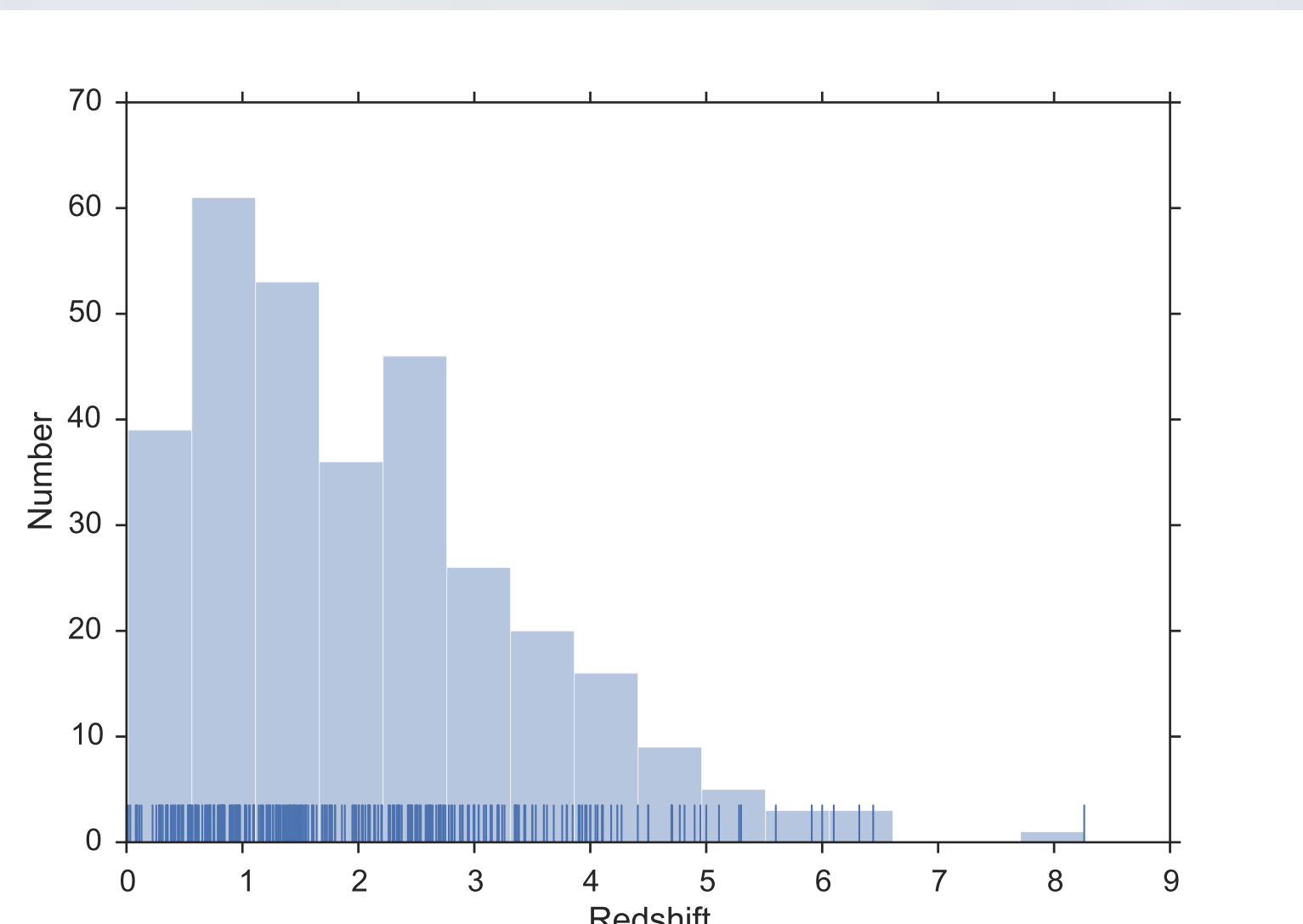
- 5) Obvious flare: luminosity at the peak of the flare must be more than double of the underlying light curve, and the signal to noise ratio (SNR) in the flare > 10

PREPARE DATA

GRBs with Known redshift

We only consider GRBs with known redshift since all our statistical analysis is done in the cosmological rest frame

Surveying 1444 GRBs observed between December 2004 and December 2016 there are **421** GRBs with known redshift.



PREPARE DATA

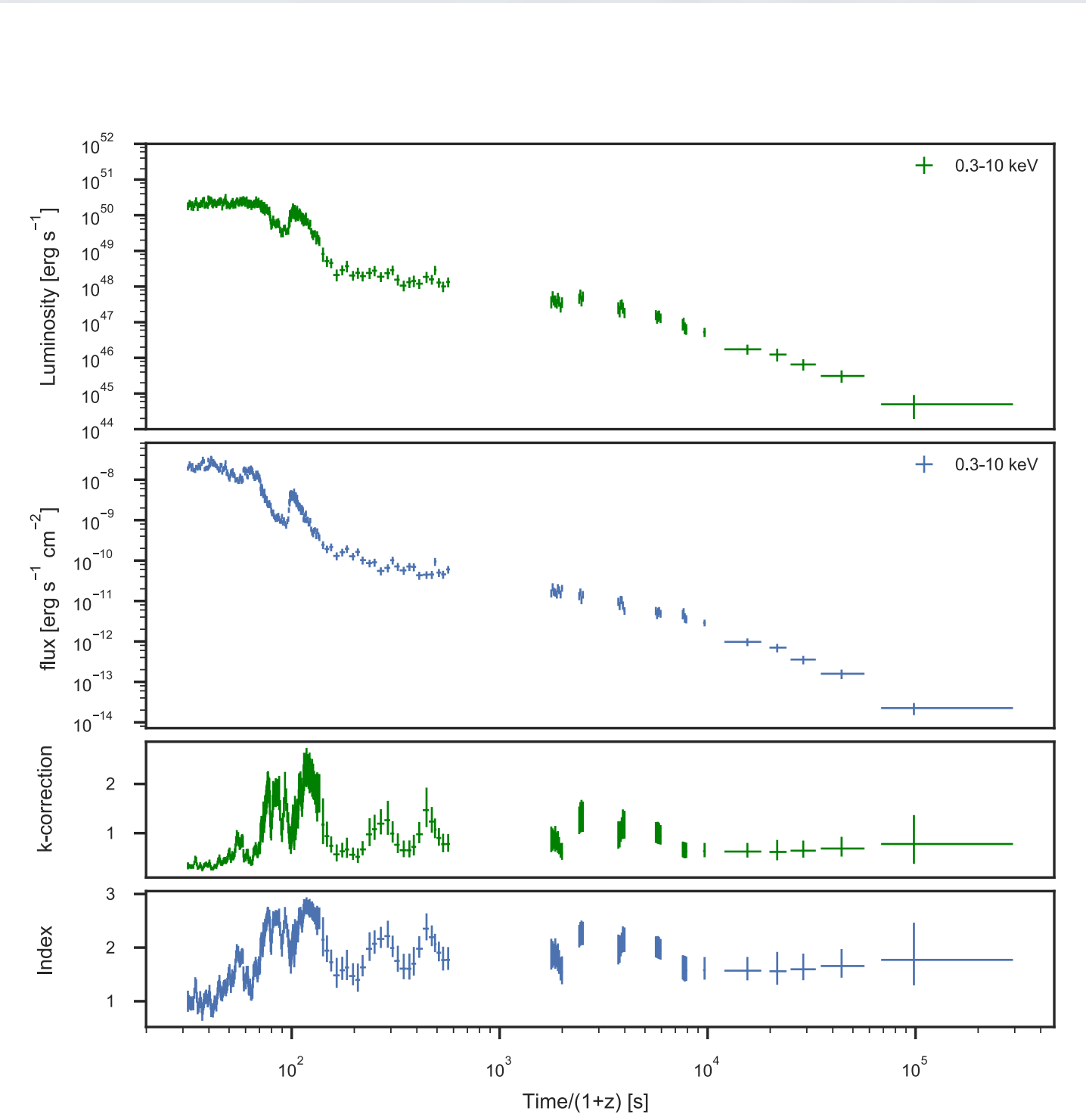
k-correction for luminosity light-curve

- Select a time bin $\delta t_{obs,i}$ centered at time $t_{obs,i}$ in the observer's frame.
- Assume a power-law spectrum and fit, normalization and power-law index found.
- Compute the k-correction and luminosity this time bin.

$$k = \frac{\int_{\epsilon_1/(1+z)}^{\epsilon_2/(1+z)} A\epsilon \left(\frac{\epsilon}{\epsilon_{pix}}\right)^{-\alpha} d\epsilon}{\int_{\epsilon_1}^{\epsilon_2} A\epsilon \left(\frac{\epsilon}{\epsilon_{pix}}\right)^{-\alpha} d\epsilon} \\ = (1+z)^{\alpha-2}$$

$$L_{[0.3,10]} = 4\pi k D_L^2 f_{obs,[0.3,10]}$$

- Perform the above steps for all the time bins to have a complete luminosity light-curve

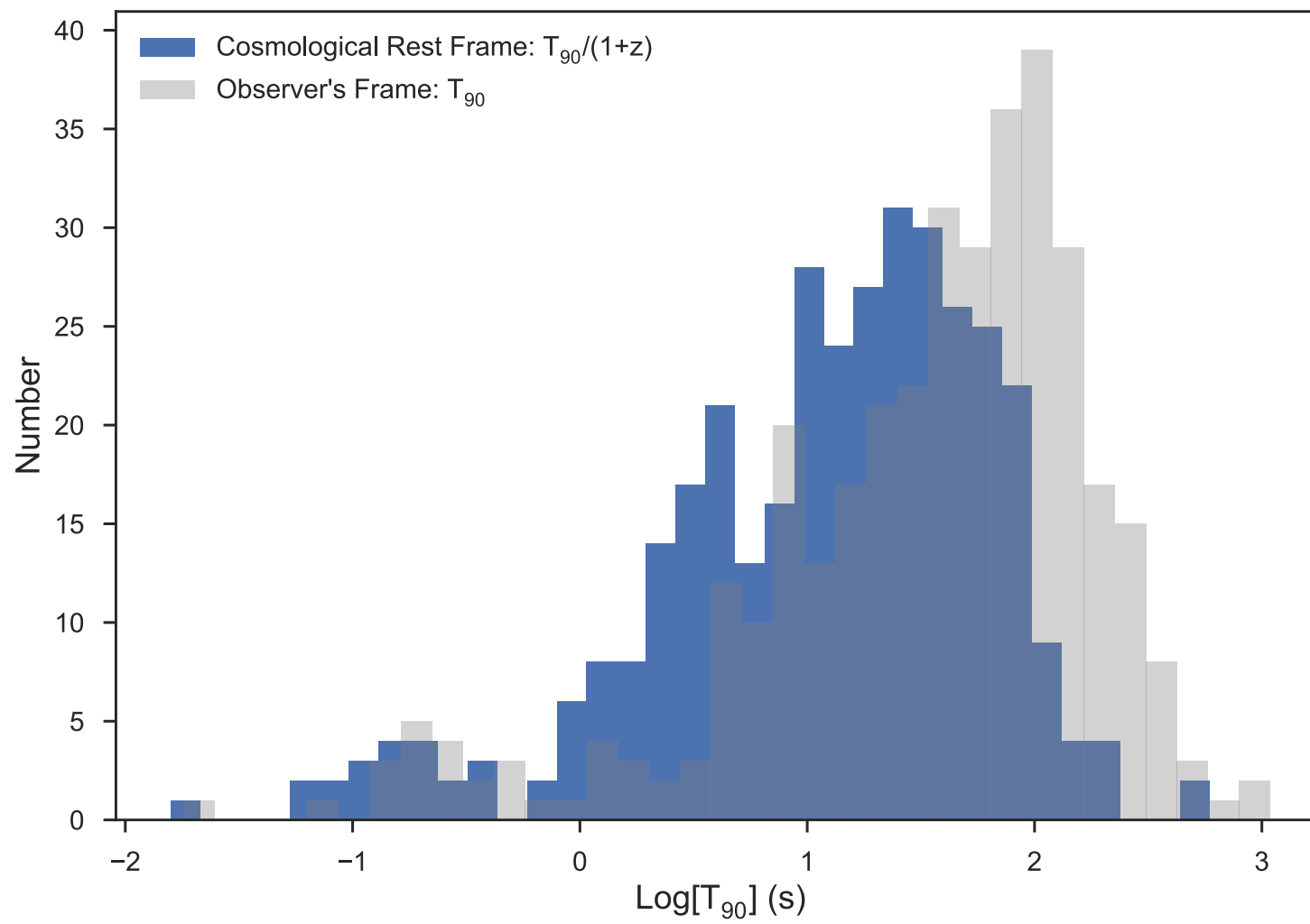


FILTER BY CRITERIA

1: Long GRB

Long and short GRBs are widely believed from different origins, we only use long GRBs of which the duration of prompt emission $T_{90} > 2$ s.

Within the 421 GRBs with known redshift, 368 GRBs have confirmed T_{90} , and 340 GRBs are long ones.

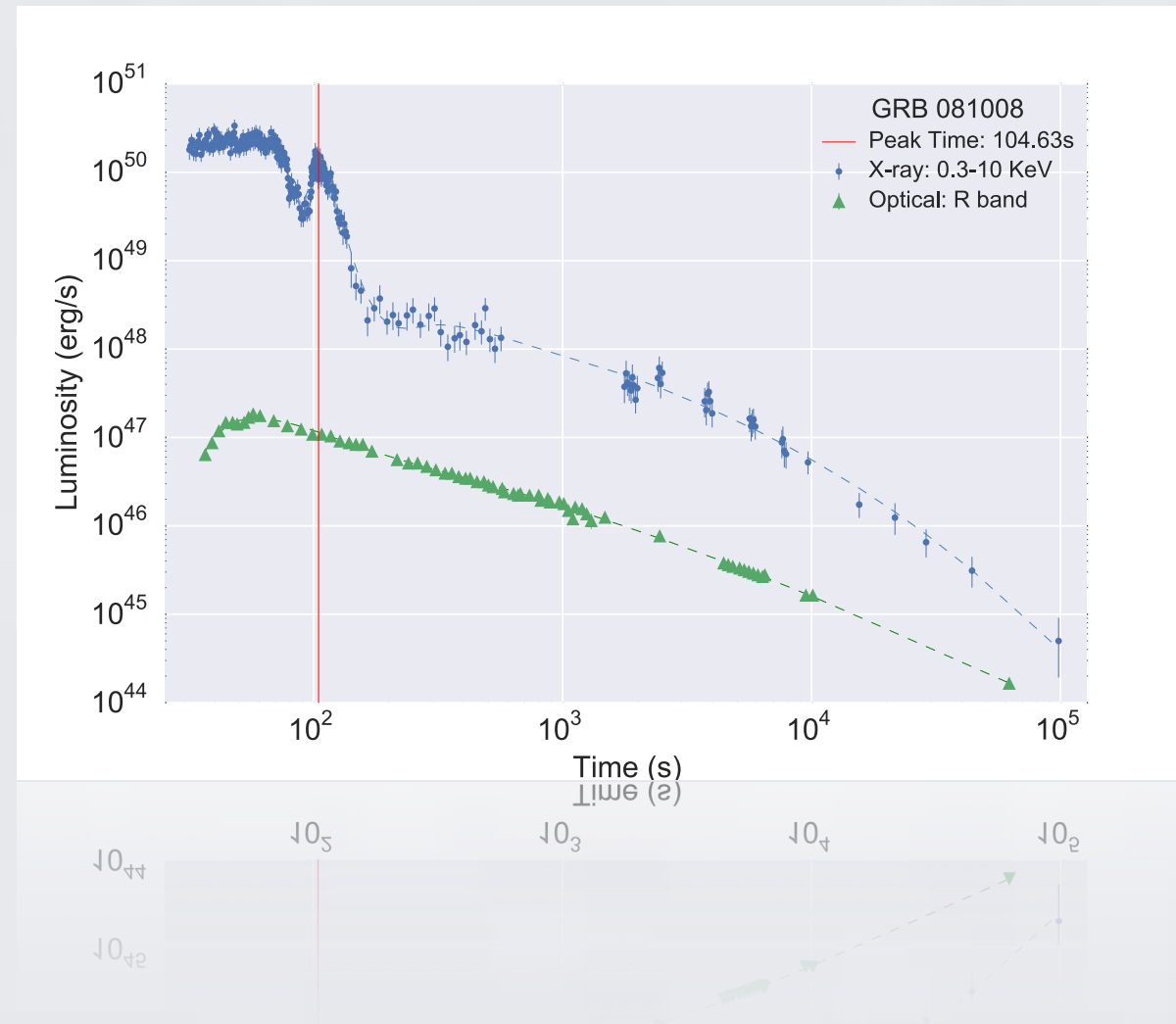


FILTER BY CRITERIA

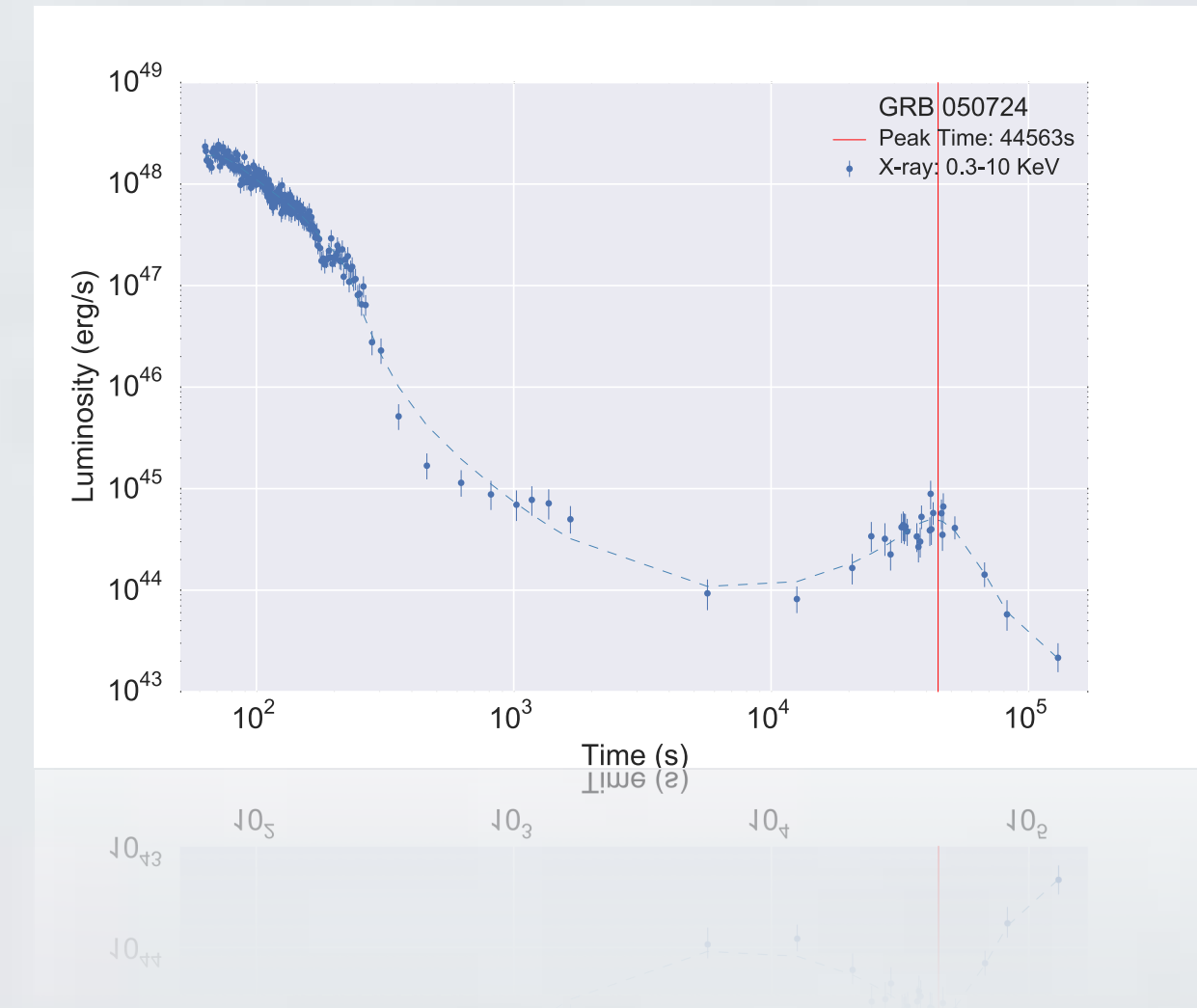
2: Flares before the plateau phase

Within 340 long GRBs, there are 211 GRBs have relatively compete Swift-XRT observation till at least one day to search for flares, and **51** GRBs are found with flares before the plateau phase.

Include



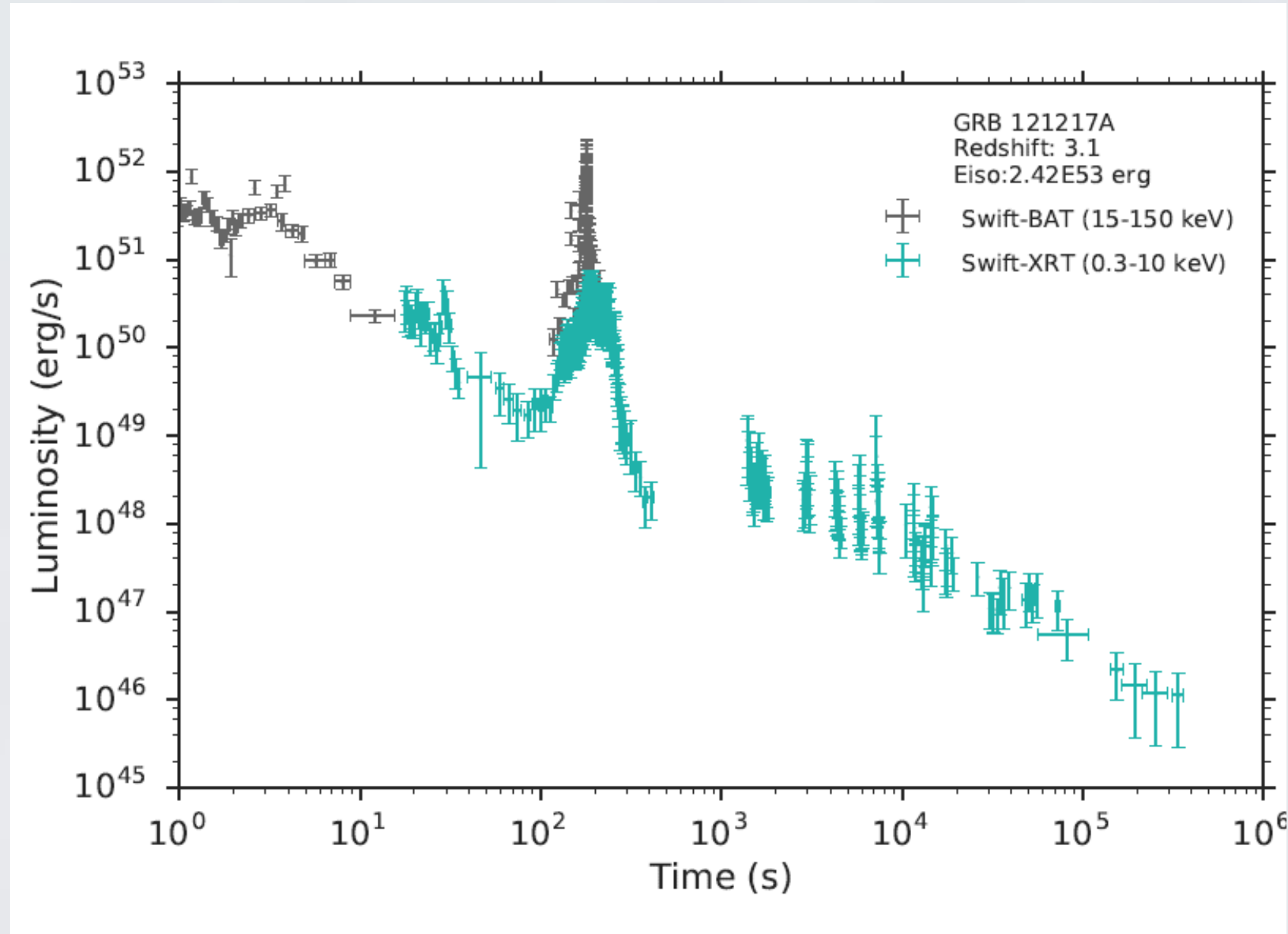
Exclude



FILTER BY CRITERIA

3: Exclude flares that other bands dominate soft X-ray band

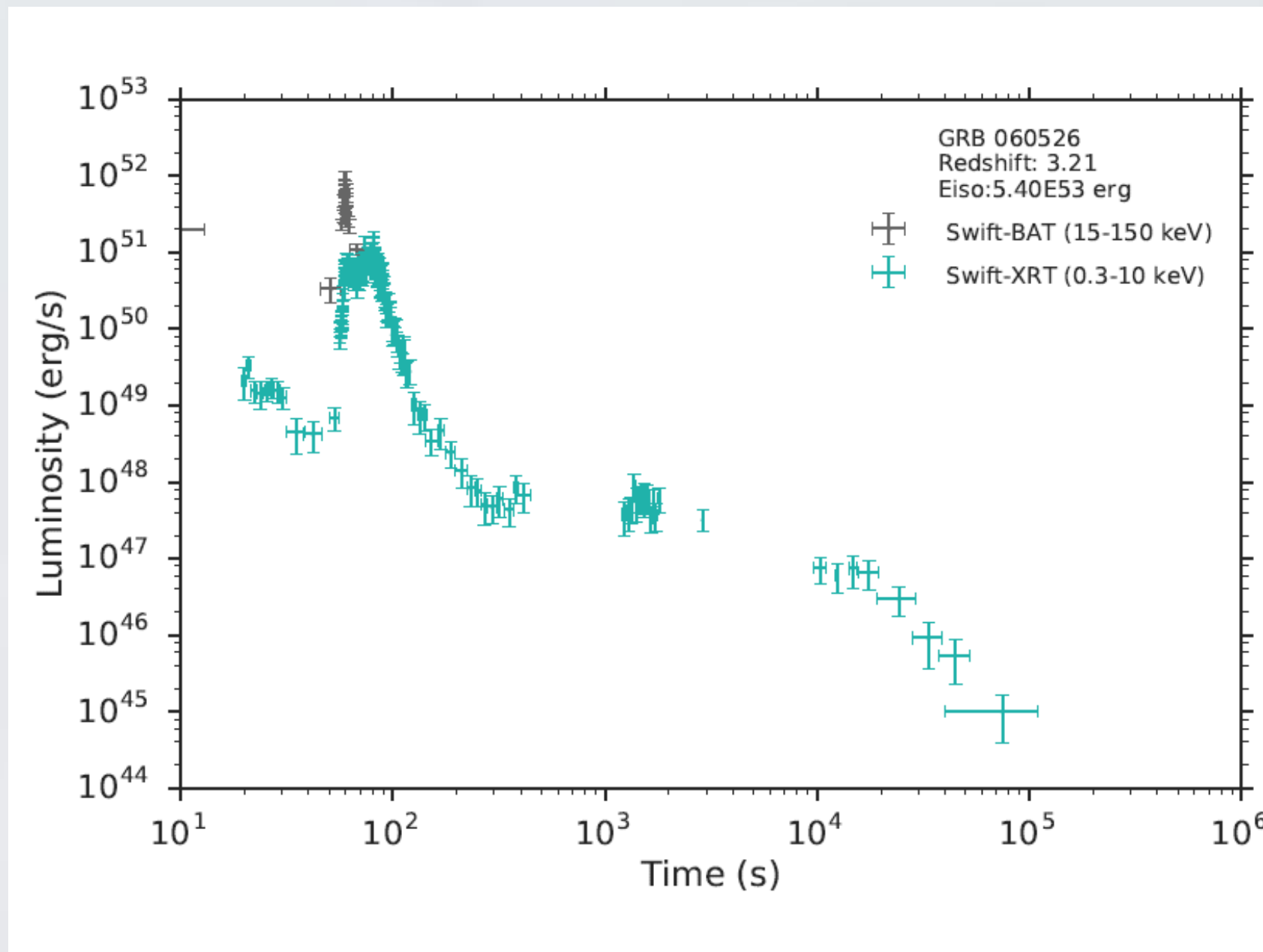
GRB 121217A clearly shows a hard X-ray counterpart which coincides with the soft X-ray flare. From the spectral analysis, the spectral index of the hard and soft X-rays evolves in a similar trend. This is an indication that the X-ray flare is likely the low energy part of a spike of the prompt emission.



FILTER BY CRITERIA

4: Exclude flares contaminated by the prompt emission

GRB 060526 exhibits two close X-ray flares. The first one has a hard X-ray counterpart and is considered to be a spike of the prompt emission. The second one is crossed and contaminated by the prompt spike.



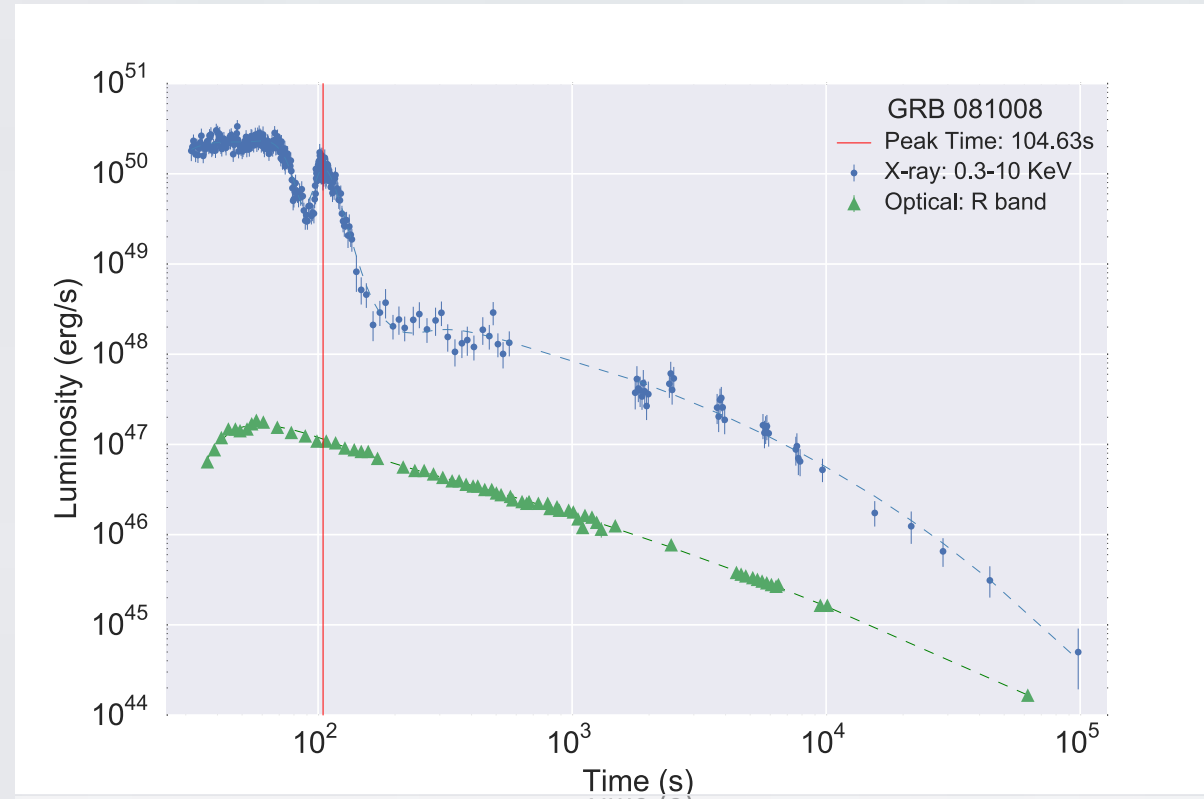
TO_T TO_S TO₃ TO₄ TO₂ TO_E Time (s)

FILTER BY CRITERIA

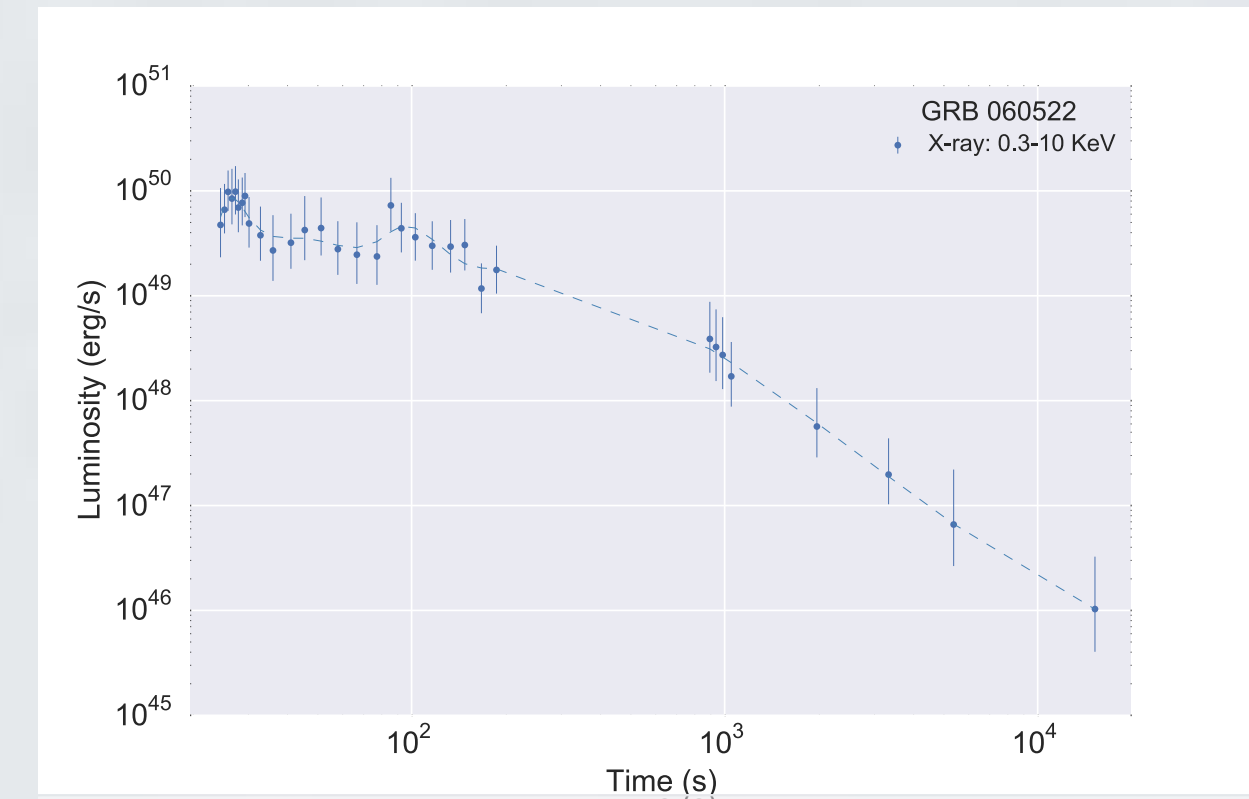
5: Obvious flares

Flares in this sample must be obvious: we select the GRBs of which luminosity must be more than double of the underlying light curve and the signal to noise ratio is higher than 20.

Include



Exclude



Locally Weighted Regression

FOR

Determining Flares

Locally weighted regression performs model fitting around a point using data weighted by the distance to that point usually the nearby data has high weight.

Local - Based on a given position x_0

Weighted - The importance (weight) of data points for the fitting is based on the distance to the given position

$$D = ae^{-\frac{||x-x_0||}{2c}}$$

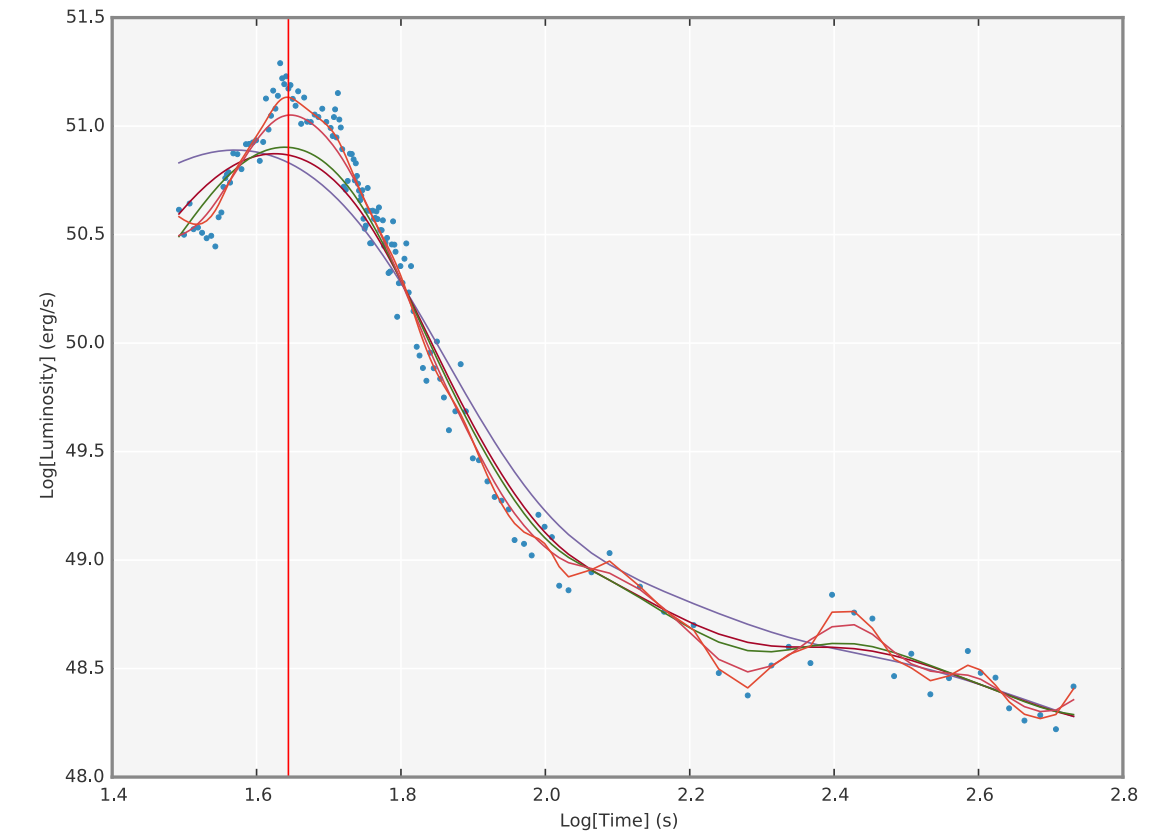
(Gaussian Kernel)

Regression - approximating a function

$$\beta = (X^T W X)^{-1} X^T W Y$$

$$y_0 = \beta x_0$$

(Linear Regression)



Code: <https://github.com/YWangScience/AstroNeuron>

K-means Clustering

FOR

Classifying and Selecting GRBs

Classifying a given data set to k clusters by minimizing the sum of difference between data

Initiation - Randomly select K cluster centers

Assignment - Assign each point to the group that has the closest center

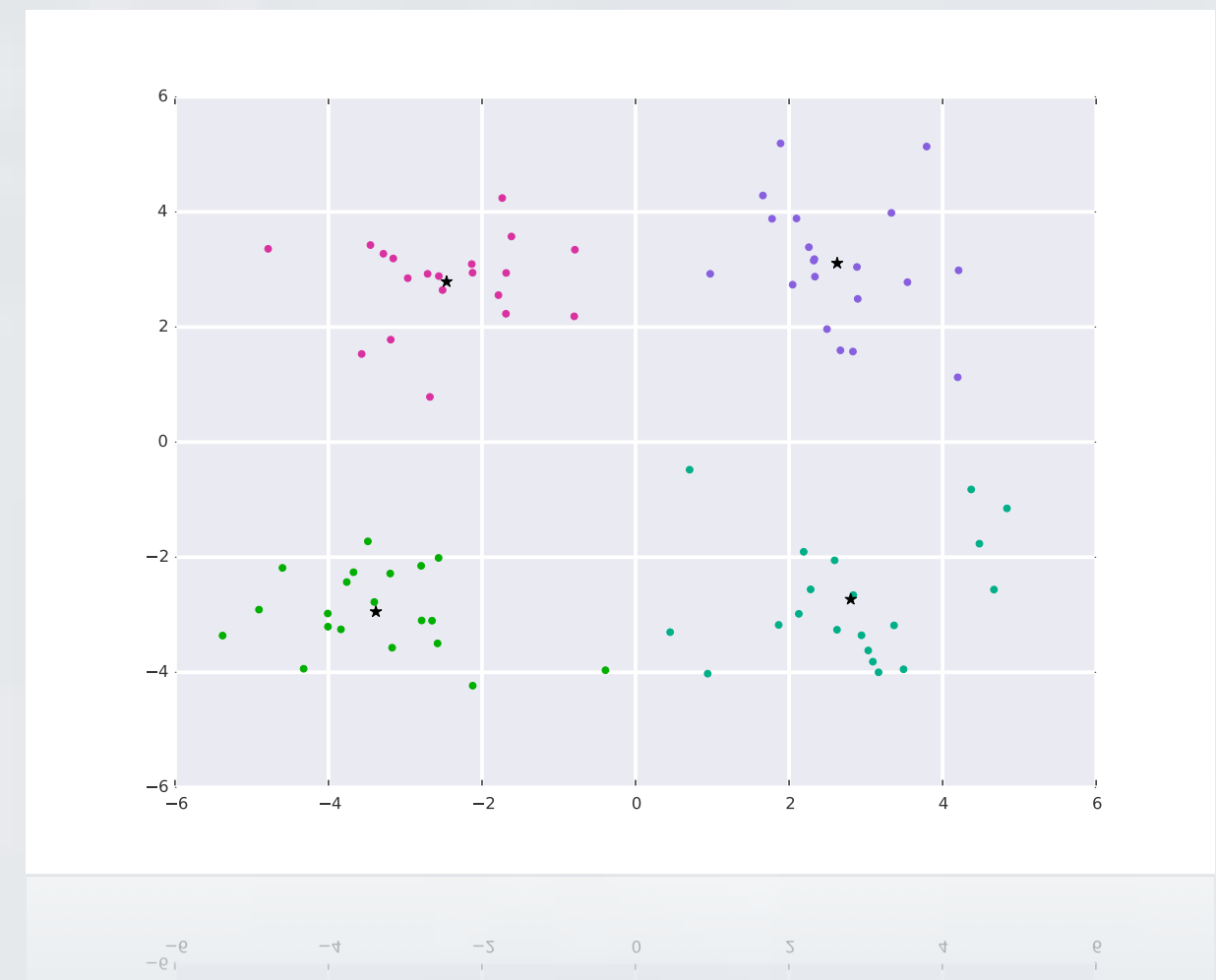
Each point (a GRB) is a n dimensional vector each dimension represents a 'selection criterion' The difference of GRBs is considered as the distance of two points (distance defined in a metric way)

Update - Recalculate the new cluster center

Mean of vectors

Repeat - Repeat **Assignment** and **Update** until the centers no longer move

$$\min \sum_{i=1}^k \sum_{x_j \in S_i} \|D(x_j, \mu_i)\|^2$$



SAMPLE SELECTION

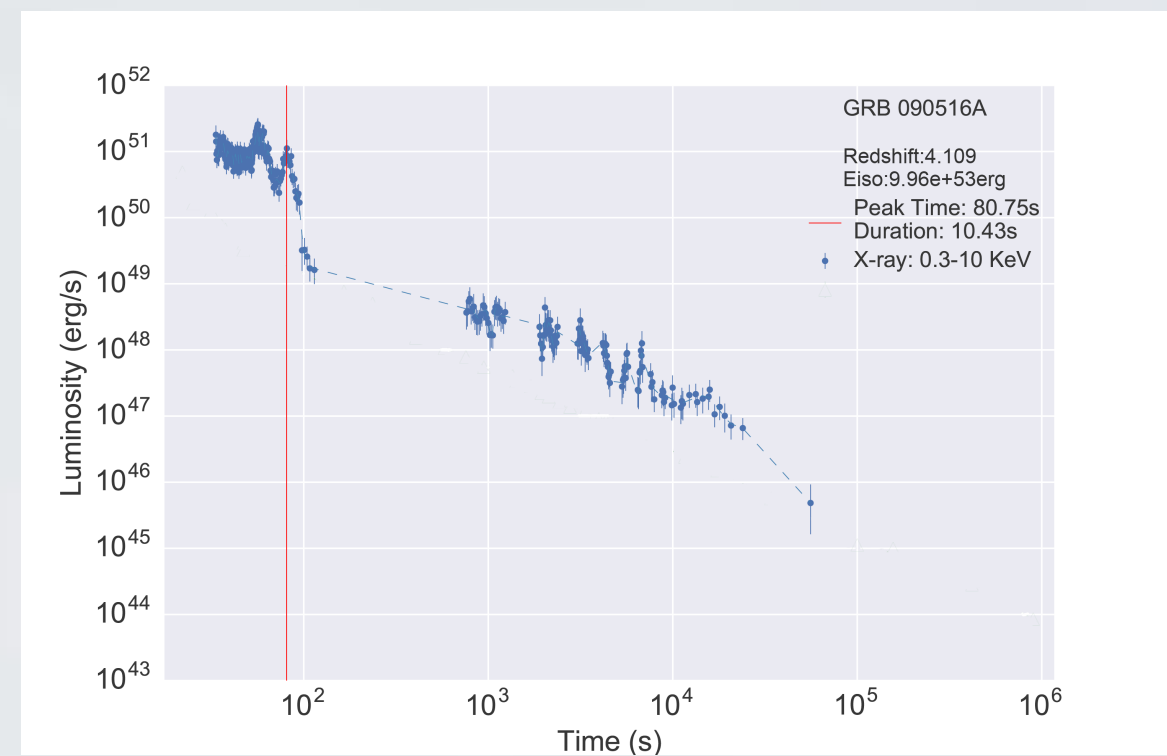
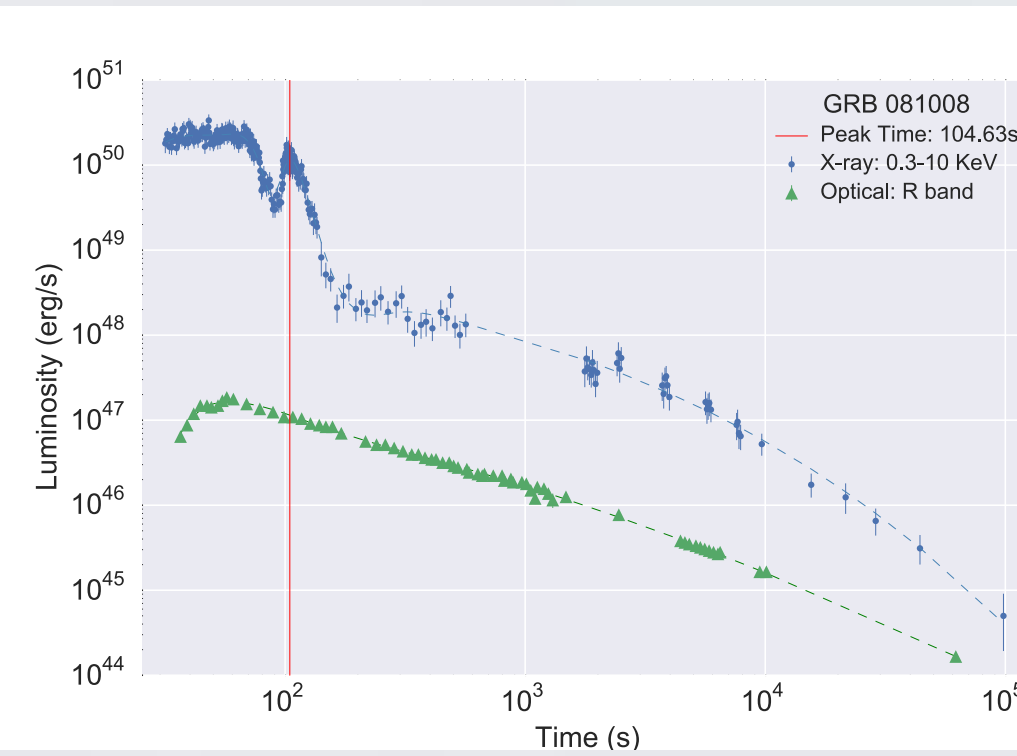
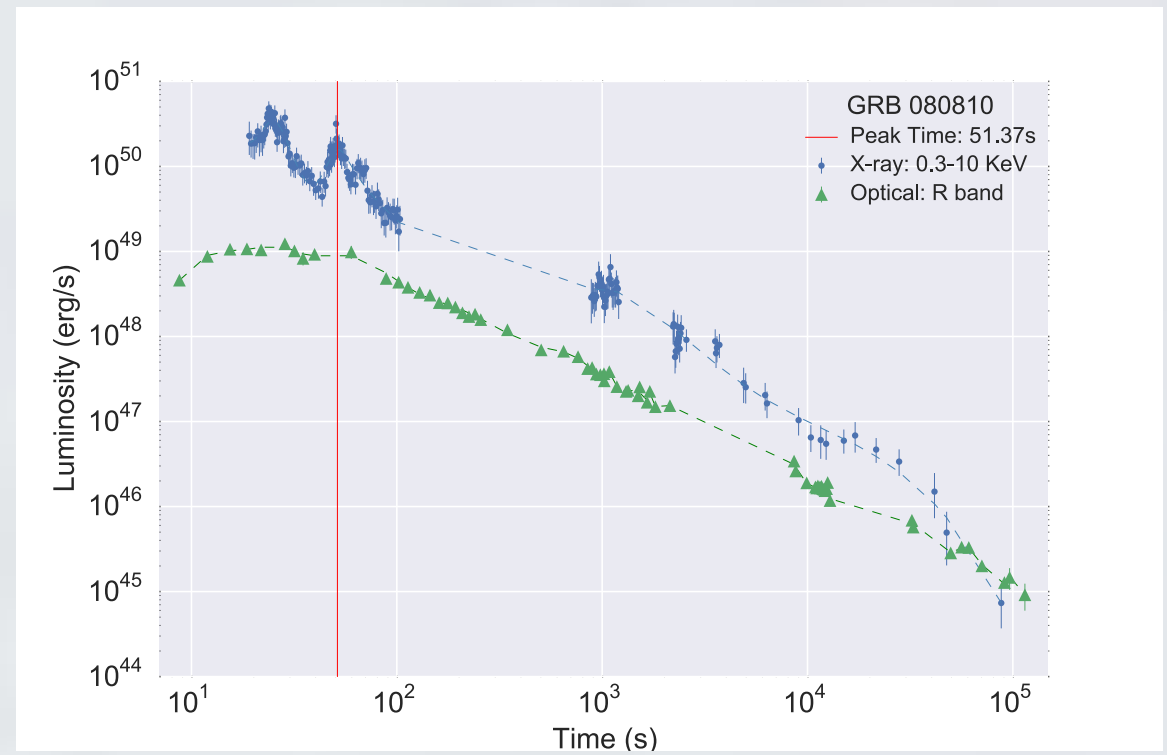
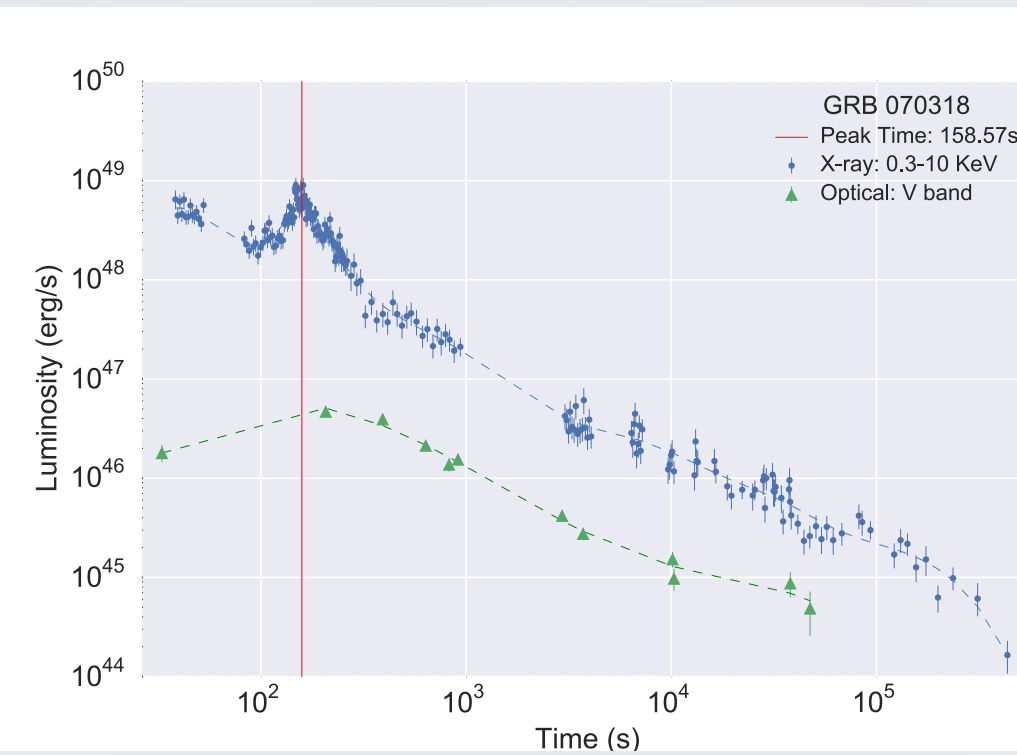
Selected Sample (16 GRBs)

GRB	z	E_{iso} (erg)	t_p (s)	L_p (erg/s)	Δt (s)	E_f (erg)
060204B	2.3393	$2.93(\pm 0.60) \times 10^{53}$	100.72 ± 6.31	$7.35(\pm 2.05) \times 10^{49}$	17.34 ± 6.83	$8.56(\pm 0.82) \times 10^{50}$
060607A	3.082	$2.14(\pm 1.19) \times 10^{53}$	66.04 ± 4.98	$2.28(\pm 0.48) \times 10^{50}$	18.91 ± 3.84	$3.33(\pm 0.32) \times 10^{51}$
070318	0.84	$3.41(\pm 2.14) \times 10^{52}$	154.7 ± 12.80	$6.28(\pm 1.30) \times 10^{48}$	63.80 ± 19.82	$3.17(\pm 0.37) \times 10^{50}$
080607	3.04	$1.87(\pm 0.11) \times 10^{54}$	37.48 ± 3.60	$1.14(\pm 0.27) \times 10^{51}$	15.63 ± 4.32	$1.54(\pm 0.24) \times 10^{52}$
080805	1.51	$7.16(\pm 1.90) \times 10^{52}$	48.41 ± 5.46	$4.66(\pm 0.59) \times 10^{49}$	27.56 ± 9.33	$9.68(\pm 1.24) \times 10^{50}$
080810	3.35	$5.00(\pm 0.44) \times 10^{53}$	51.03 ± 6.49	$1.85(\pm 0.53) \times 10^{50}$	12.38 ± 4.00	$1.80(\pm 0.17) \times 10^{51}$
081008	1.967	$1.35(\pm 0.66) \times 10^{53}$	102.24 ± 5.66	$1.36(\pm 0.33) \times 10^{50}$	18.24 ± 3.63	$1.93(\pm 0.16) \times 10^{51}$
081210	2.0631	$1.56(\pm 0.54) \times 10^{53}$	127.59 ± 13.68	$2.23(\pm 0.21) \times 10^{49}$	49.05 ± 6.49	$8.86(\pm 0.54) \times 10^{50}$
090516A	4.109	$9.96(\pm 1.67) \times 10^{53}$	80.75 ± 2.20	$9.10(\pm 2.26) \times 10^{50}$	10.43 ± 2.44	$7.74(\pm 0.63) \times 10^{51}$
090812	2.452	$4.40(\pm 0.65) \times 10^{53}$	77.43 ± 16.6	$3.13(\pm 1.38) \times 10^{50}$	17.98 ± 4.51	$5.18(\pm 0.61) \times 10^{51}$
131030A	1.293	$3.00(\pm 0.20) \times 10^{53}$	49.55 ± 7.88	$6.63(\pm 1.12) \times 10^{50}$	33.73 ± 6.55	$3.15(\pm 0.57) \times 10^{52}$
140206A	2.73	$3.58(\pm 0.79) \times 10^{53}$	62.11 ± 12.26	$4.62(\pm 0.99) \times 10^{50}$	26.54 ± 4.31	$1.04(\pm 0.59) \times 10^{51}$
140301A	1.416	$9.50(\pm 1.75) \times 10^{51}$	276.56 ± 15.50	$5.14(\pm 1.84) \times 10^{48}$	64.52 ± 10.94	$3.08(\pm 0.22) \times 10^{50}$
140419A	3.956	$1.85(\pm 0.77) \times 10^{54}$	41.00 ± 4.68	$6.23(\pm 1.45) \times 10^{50}$	14.03 ± 5.74	$7.22(\pm 0.88) \times 10^{51}$
141221A	1.47	$6.99(\pm 1.98) \times 10^{52}$	140.38 ± 5.64	$2.60(\pm 0.64) \times 10^{49}$	38.34 ± 9.26	$7.70(\pm 0.78) \times 10^{50}$
151027A	0.81	$3.94(\pm 1.33) \times 10^{52}$	183.79 ± 16.43	$7.10(\pm 1.75) \times 10^{48}$	163.5 ± 30.39	$4.39(\pm 2.91) \times 10^{51}$

AETFOAT	3.826	$1.80(\pm 0.77) \times 10^{51}$	47.00 ± 00.48	$8.04(\pm 4.42) \times 10^{49}$	47.2 ± 30.41	$4.55(\pm 2.22) \times 10^{51}$
AT2021AT	0.0	$3.01(\pm 1.33) \times 10^{52}$	183.79 ± 16.43	$7.10(\pm 1.75) \times 10^{48}$	163.5 ± 30.39	$4.39(\pm 2.91) \times 10^{51}$
AT2021AT	0.0	$3.01(\pm 1.33) \times 10^{52}$	183.79 ± 16.43	$7.10(\pm 1.75) \times 10^{48}$	163.5 ± 30.39	$4.39(\pm 2.91) \times 10^{51}$
AT2021AT	0.0	$3.01(\pm 1.33) \times 10^{52}$	183.79 ± 16.43	$7.10(\pm 1.75) \times 10^{48}$	163.5 ± 30.39	$4.39(\pm 2.91) \times 10^{51}$
AT2021AT	0.0	$3.01(\pm 1.33) \times 10^{52}$	183.79 ± 16.43	$7.10(\pm 1.75) \times 10^{48}$	163.5 ± 30.39	$4.39(\pm 2.91) \times 10^{51}$

X-RAY FLARE

Sample: Examples



X-RAY FLARES

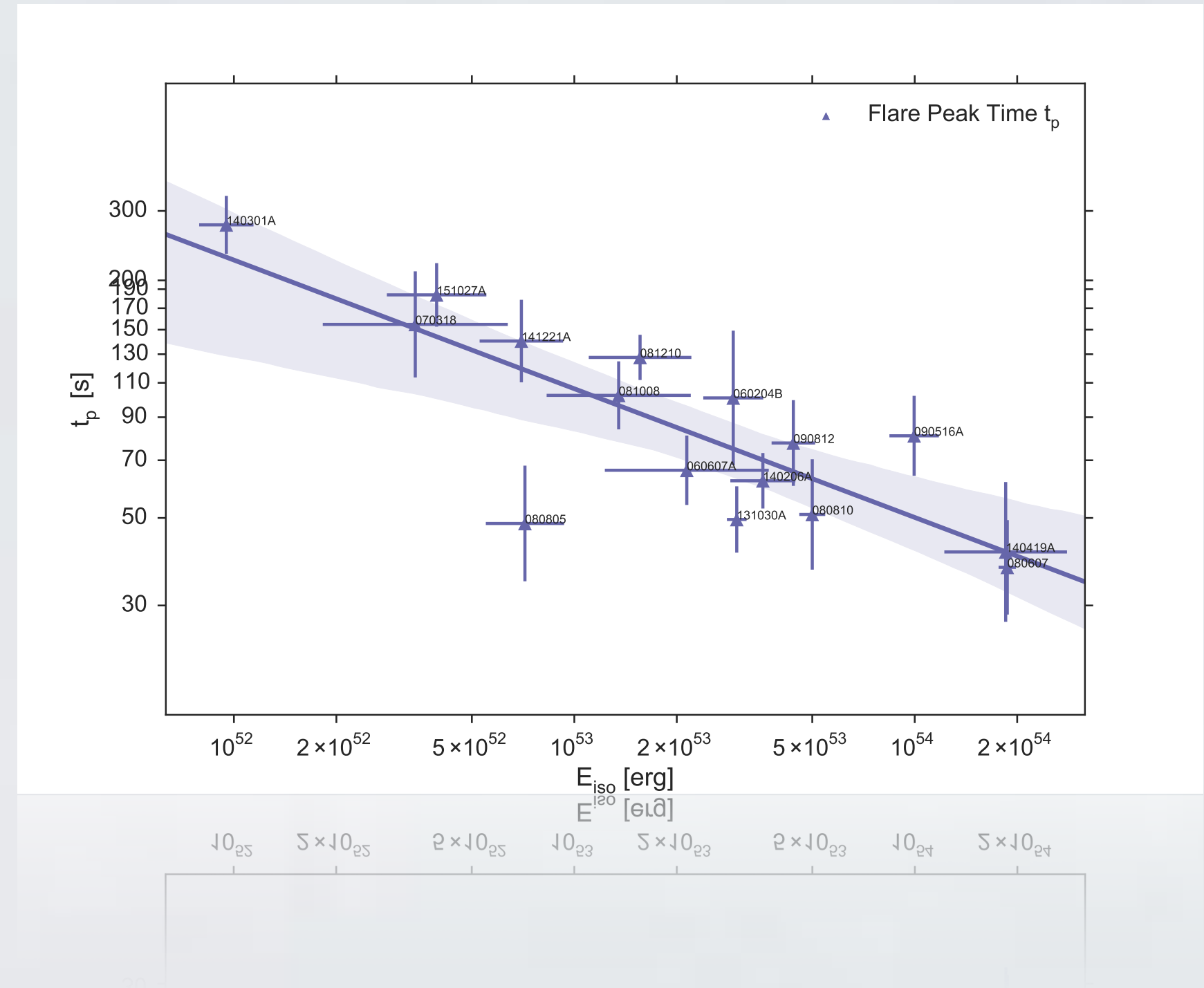
STATISTIC

CORRELATION

$E_{\text{iso}} - t_p$ (Isotropic Energy - Flare Peak Time)

The relation between the isotropic energy E_{iso} and the peak time of X-ray flare t_p . The starting time t_0 is considered as the trigger time t_{trigger} of Swift satellite.

This figure is plotted in logarithm all the value are in the rest frame, the straight lines are the power-fitting the shadows indicate the 95% confidence level.



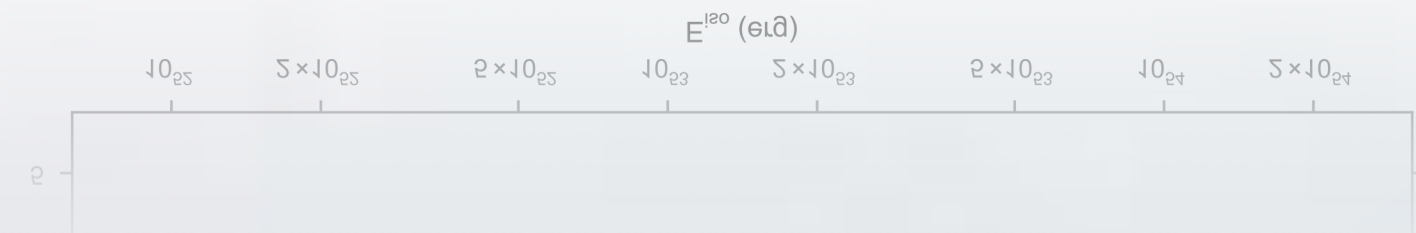
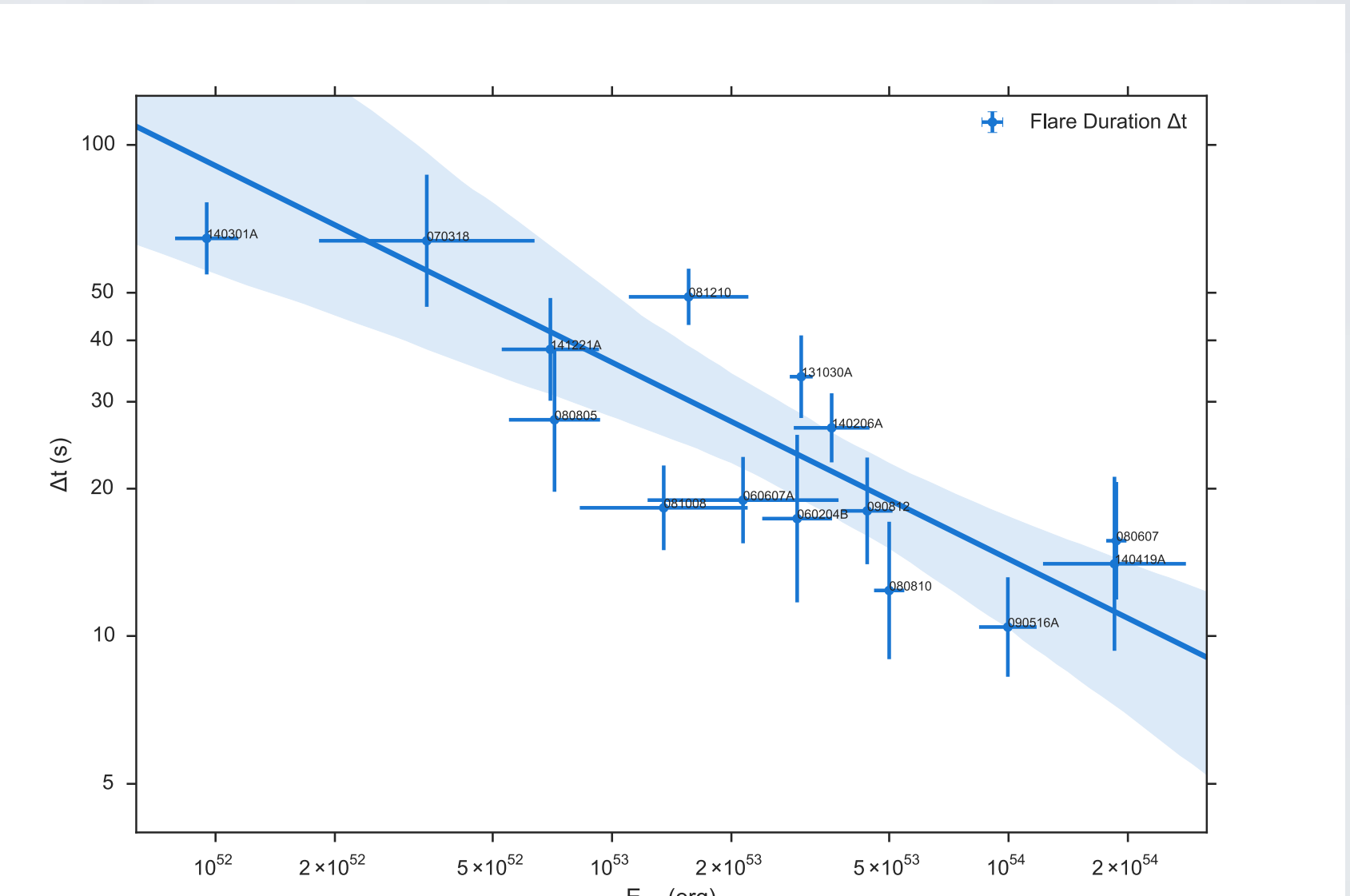
CORRELATION

$E_{\text{iso}} - \Delta t$ (*Isotropic Energy - Flare Duration*)

The relation between the isotropic energy E_{iso} and the duration of flare Δt .

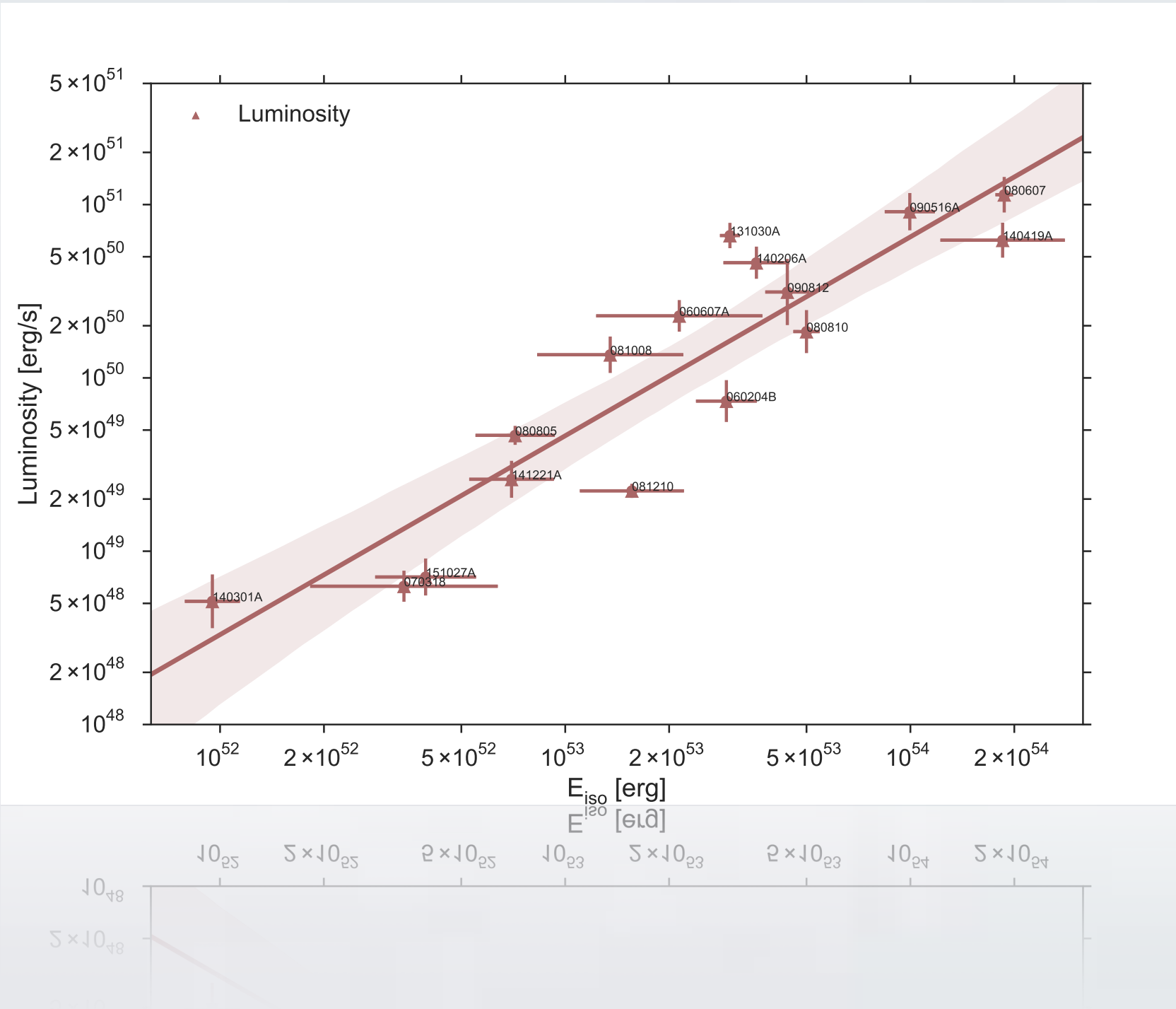
Here Δt is defined as the width of the X-ray flare the starting and ending time correspond to half luminosity of the peak time.

This figure is plotted in logarithm all the value are in the rest frame, the straight lines are the power-fitting the shadows indicate the 95% confidence level.



CORRELATION

$E_{\text{iso}} - L_p$ (Isotropic Energy - Peak Luminosity)

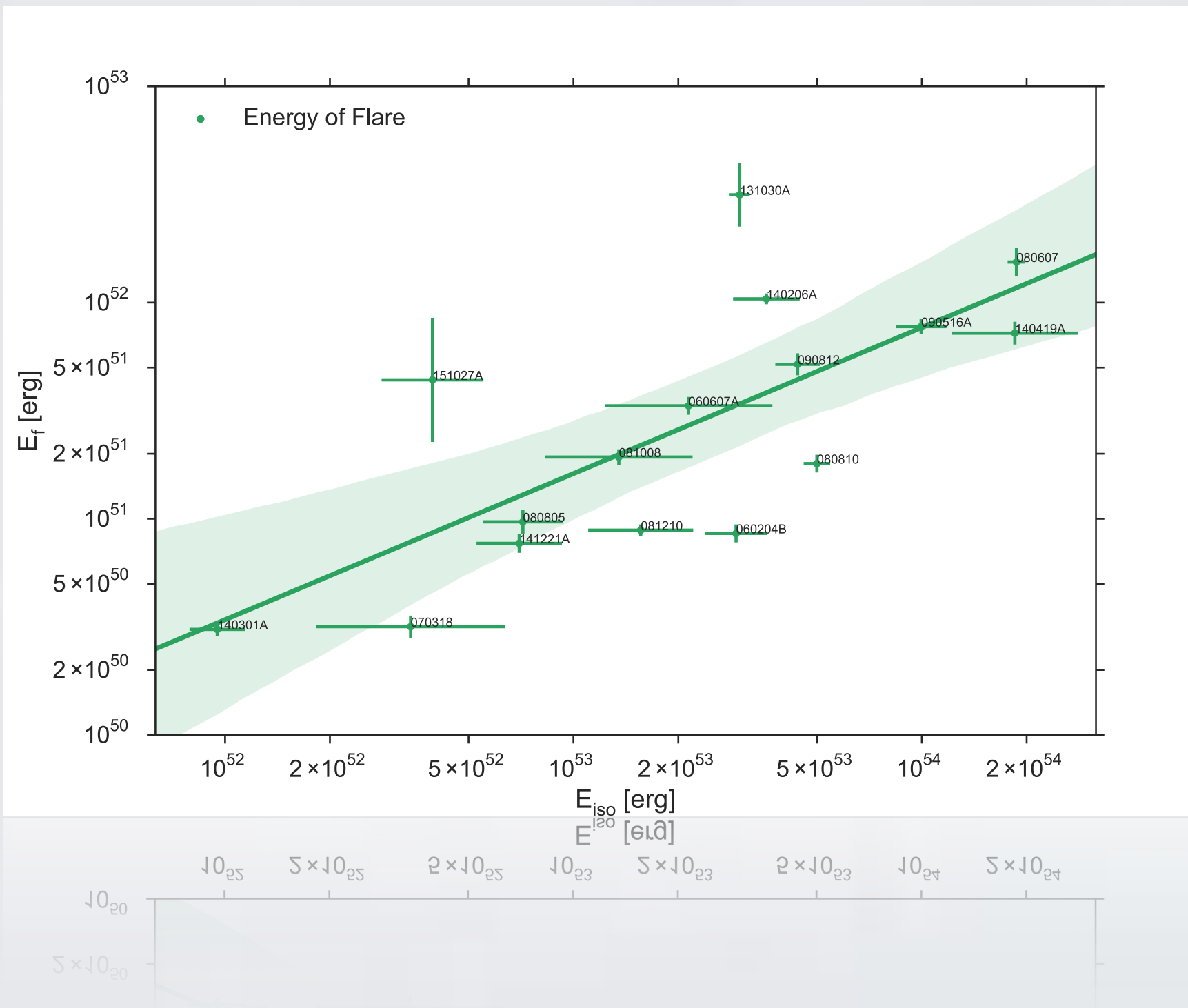


The relation between the isotropic energy E_{iso} and luminosity at the peak of the flare L_p .

Plotted in logarithm value are in the rest frame the straight line indicates a power-law fitting the shadow covers 95% confidence level.

CORRELATION

$E_{\text{iso}} - E_{\text{flare}}$ (*Isotropic Energy - Flare Energy*)



The relation between the isotropic energy E_{iso} and the energy in the X-ray flare E_{flare} .

Plotted in logarithm value are in the rest frame the straight line indicates a power-law fitting the shadow covers 95% confidence level.

CORRELATION

Correlation Fitted by MCMC

Power-law correlations among the quantities. The values and uncertainties (1-sigma) of the power-law index and of the correlation coefficient are obtained from 10^5 Markov chain Monte Carlo (MCMC) iterations. All relations are highly correlated, the E_{iso} - L_p has the highest correlation coefficient.

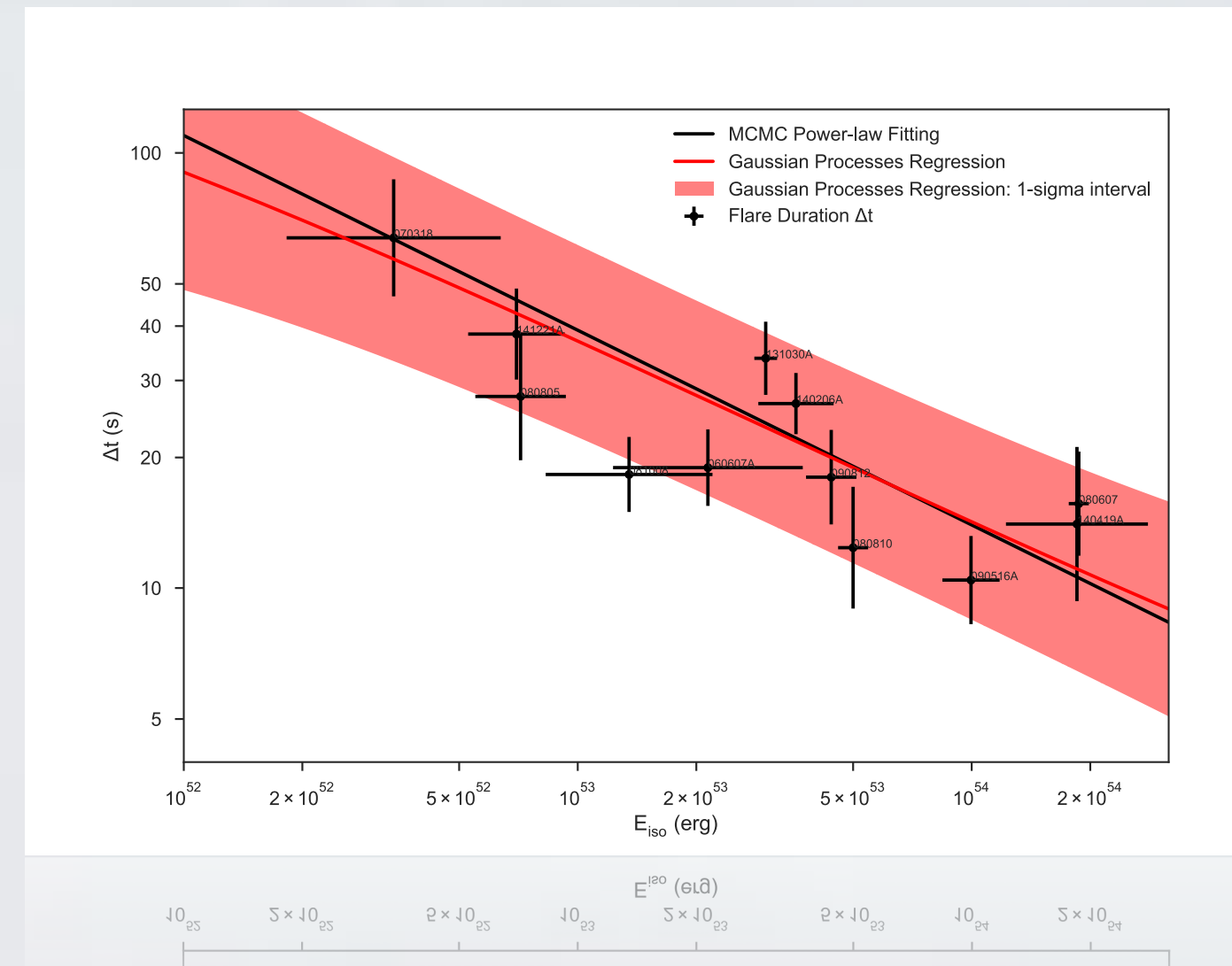
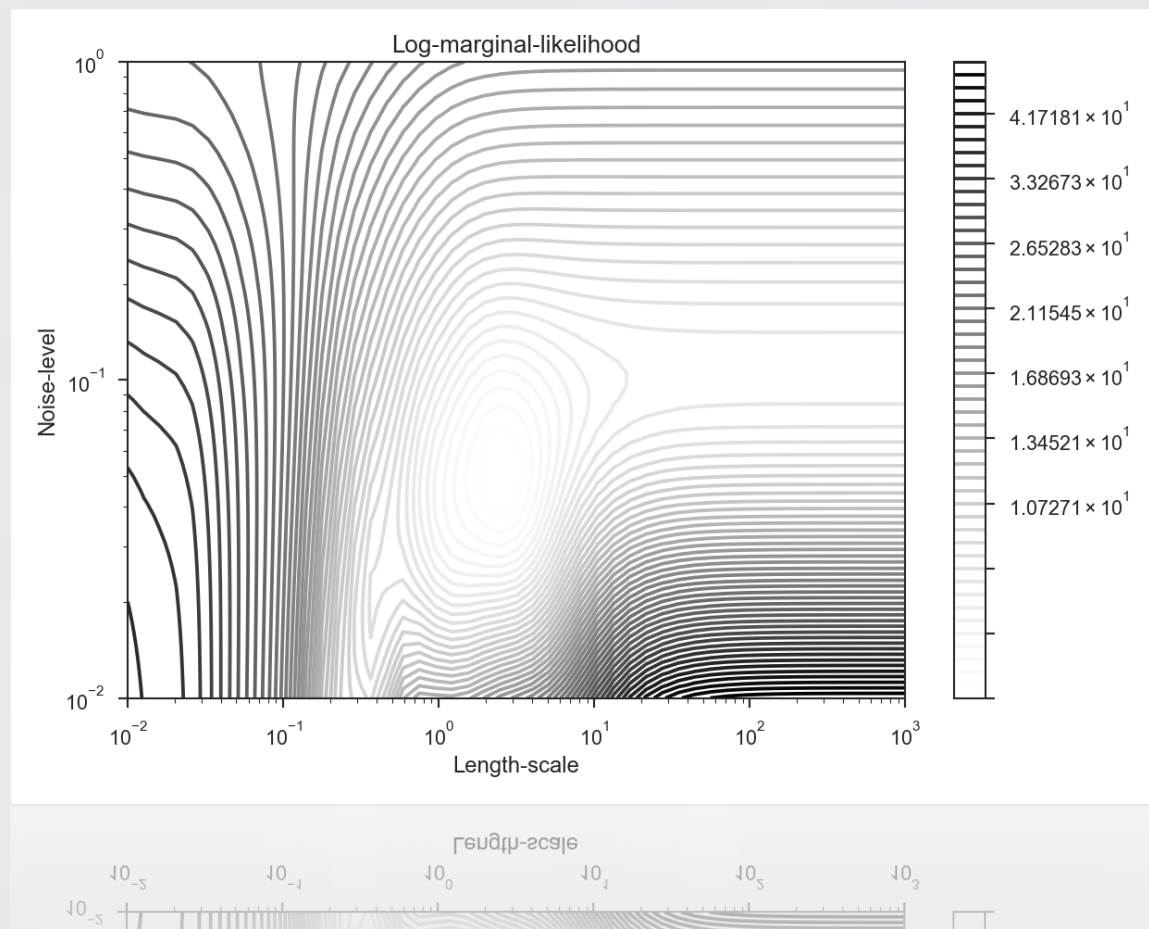
Correlation	Power-Law Index	Coefficient
$E_{iso} - t_p$	$-0.290(\pm 0.010)$	$-0.764(\pm 0.123)$
$E_{iso} - \Delta t$	$-0.461(\pm 0.042)$	$-0.760(\pm 0.138)$
$E_{iso} - L_p$	$1.186(\pm 0.037)$	$0.883(\pm 0.070)$
$E_{iso} - E_f$	$0.631(\pm 0.117)$	$0.699(\pm 0.145)$
$E_{iso} - E^t$	$1.11.0(\pm 0.039)$	$0.663(\pm 0.142)$
$E_{iso} - \Gamma^b$	$1.180(\pm 0.031)$	$0.883(\pm 0.100)$

CORRELATION

Verify by Gaussian Process Regression (GPR)

Left: GPR marginal likelihood, the minimal value locates at noise level $\sim 8\%$. This noise could be induced from other parameters that effect the Eiso and Δt , for instance, the speed, the shape of the emitter, the measurement uncertainty, and etc..

Right: The GPR fitted curve and its 1-sigma region in red, and the power-law fitting by MCMC in black. The GPR curve almost coincides with the power-law line, which indicates the power-law assumption is appropriate.



CORRELATION

Correlations Inference

Previous explanation of X-ray flares: activity of the GRB central engine

- 1) The central engine produces a series of outgoing shells with a variety of independent Lorentz factors, the collisions between these shells occur over a wide time range, producing the prompt emission and the X-ray flares.
- 2) The prompt emission and flares are emitted from the photospheres with different Lorentz factors.
- 3) Produced by the continuous or discrete accretion from a surrounding disk.

All of these models expect the prompt emission and the afterglow are similar entities but arise independently.

This stochasticity in principle shall lead to the independency of observational quantities between the prompt emission and the X-ray flare, and no correlation shall be found.

But at least for our sample, the prompt emission and the X-ray flare are strictly correlated.

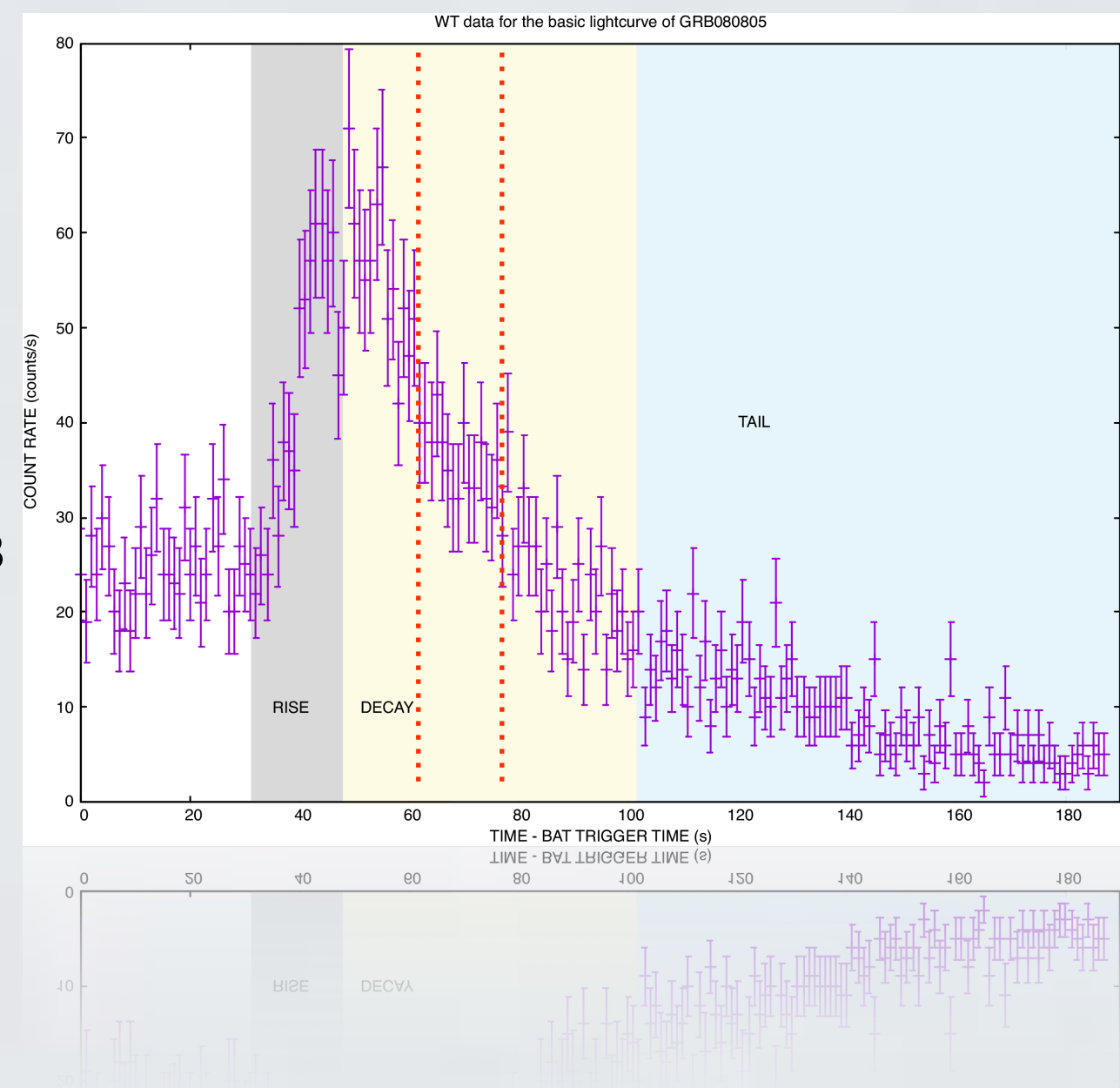
X-RAY FLARES

THERMAL
COMPONENT

THERMAL COMPONENT

Split Time Intervals

- At least two bins A and B A is the rising part of flare
B is the decaying part of flare.
- If there is a flat part C C is taken as one bin.
- Split A and B to small bins (A1 A2 B1 B2 ...) with following criteria
 - At least 200 counts per bin
 - Signal to noise ratio > 20
- If the PC data in A or in B doesn't conform to the above criteria take all the PC data in A or in B as one bin.



THERMAL COMPONENT

Compare Models

Data Distribution - We have a spectrum extracted from a GRB in a given time range and the spectrum is composed of several bins. In each bin (eg. ***i*th** bin) from the assumed theoretical model we shall observe \mathbf{M}_i counts of photons and from the observation we see \mathbf{D}_i counts of photons. From the Poisson distribution which is generally valid for X-ray observation the possibility of finding \mathbf{D}_i counts if predicted \mathbf{M}_i counts in ***i*th** bin is

$$P(D_i|M_i) = \frac{M_i^{D_i}}{D_i!} e^{-M_i}$$

Model Fitting - For X-ray astronomy it is usual to maximize the likelihood defined by W. Cash namely the C-statistic

$$C = -2 \ln \prod_{i=1}^N P(D_i|M_i)$$

Compare Nested Model - nested means one model (full model) has one or more additional terms adding on the other model (reduced model). Maximum likelihood ratio (MLR) method is used to compare models fitted by Cash statistic

$$\text{SIG}_{\text{MLR}} = \int_{\Delta C}^{\infty} P(\Delta C'|\Delta \text{DOF}) d\Delta C' = \int_{\Delta C}^{\infty} \frac{2^{-\frac{\Delta \text{DOF}}{2}} e^{-\frac{\Delta C'}{2}} \Delta C'^{\frac{\Delta \text{DOF}}{2}-1}}{\Gamma\left(\frac{\Delta \text{DOF}}{2}\right)} d\Delta C'$$
$$\text{DOF} = N - k - 1$$

where DOF is the degree of freedom N is the data number k is the parameter number.

THERMAL COMPONENT

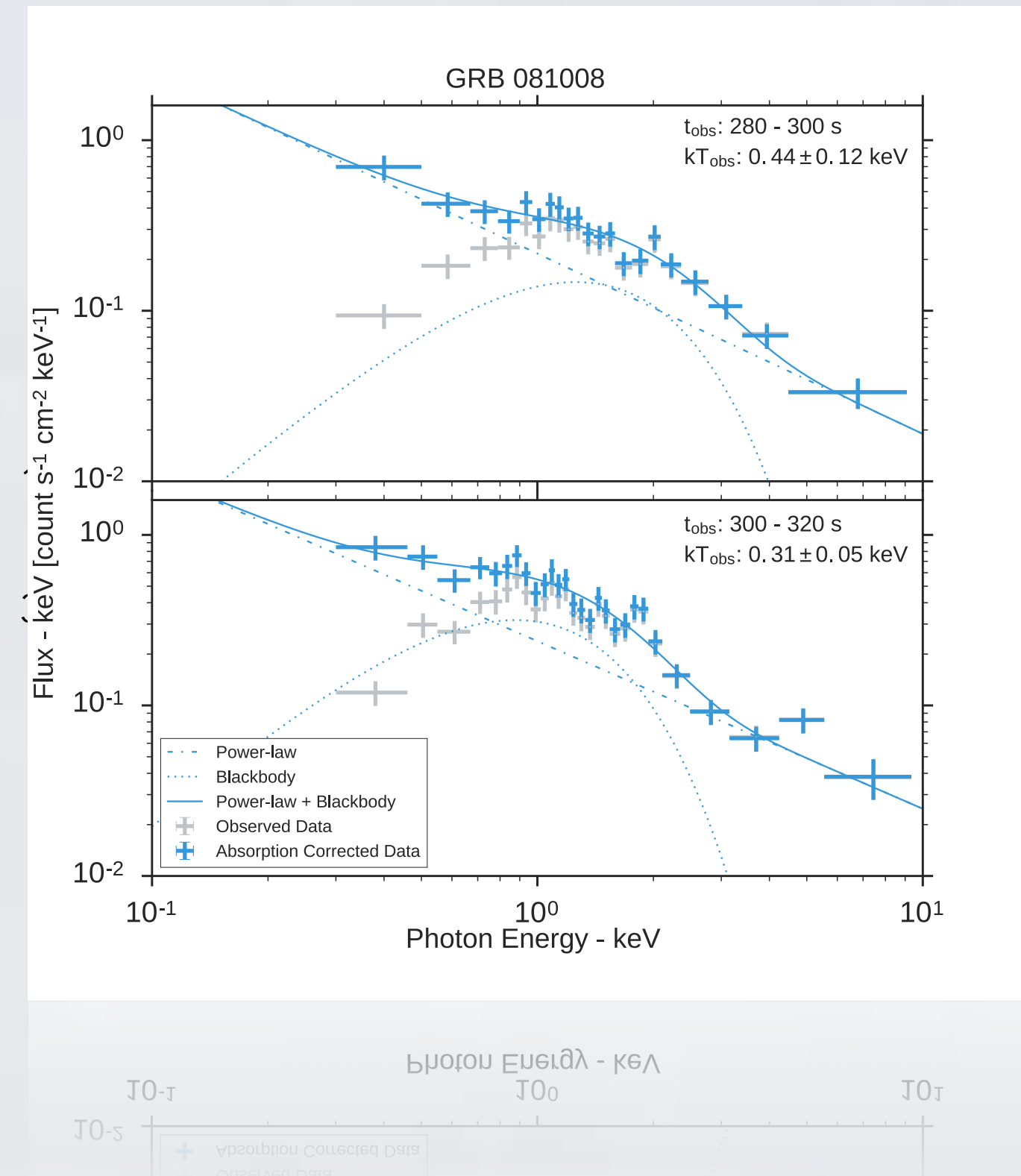
High Confidence Thermal Component (7/16 GRBs)

080805 ($Z = 1.51$)

FLARE REGION	TIME	KT	SIG
Rise	100 - 117	0.70 (0.42)	0.244
Decay	117 - 127	0.60 (0.08)	0.999
Decay	127 - 137	0.47 (0.23)	0.994
Decay	137 - 167	1.19 (0.18)	0.921
Decay	167 - 247	0.14 (0.03)	0.993

090516A ($Z = 4.109$)

FLARE REGION	TIME	KT	SIG
Rise	218 - 274	0.61 (0.04)	0.999
Decay	274 - 289	0.57 (0.04)	0.999
Decay	289 - 302	0.43 (0.06)	0.999
Decay	302 - 343	0.15 (0.03)	0.950



THERMAL COMPONENT

Analytical Computation

Averaged effective temperature:

$$T_{\text{obs}}(T_{\text{com}}, z, \Gamma) = \frac{1}{1+z} \frac{\int_{\beta}^1 \mathcal{D}(\cos \vartheta) T_{\text{com}} \cos \vartheta d \cos \vartheta}{\int_{\beta}^1 \cos \vartheta d \cos \vartheta} = \Theta(\beta) \frac{\Gamma}{1+z} T_{\text{com}}$$

$$\Theta(\beta) \equiv 2 \frac{\beta(\beta - 1) + \ln(1 + \beta)}{\beta^2}$$

Infer the radius of the thermal emitter:

$$R_{\text{lab}} = \Theta(\beta)^2 \Gamma \frac{D_L(z)}{(1+z)^2} \sqrt{\frac{F_{\text{bb,obs}}}{\sigma T_{\text{obs}}^4}} = \Theta(\beta)^2 \Gamma R_{\text{nonrel}}$$

Compute the velocity of expansion from the change of radius:

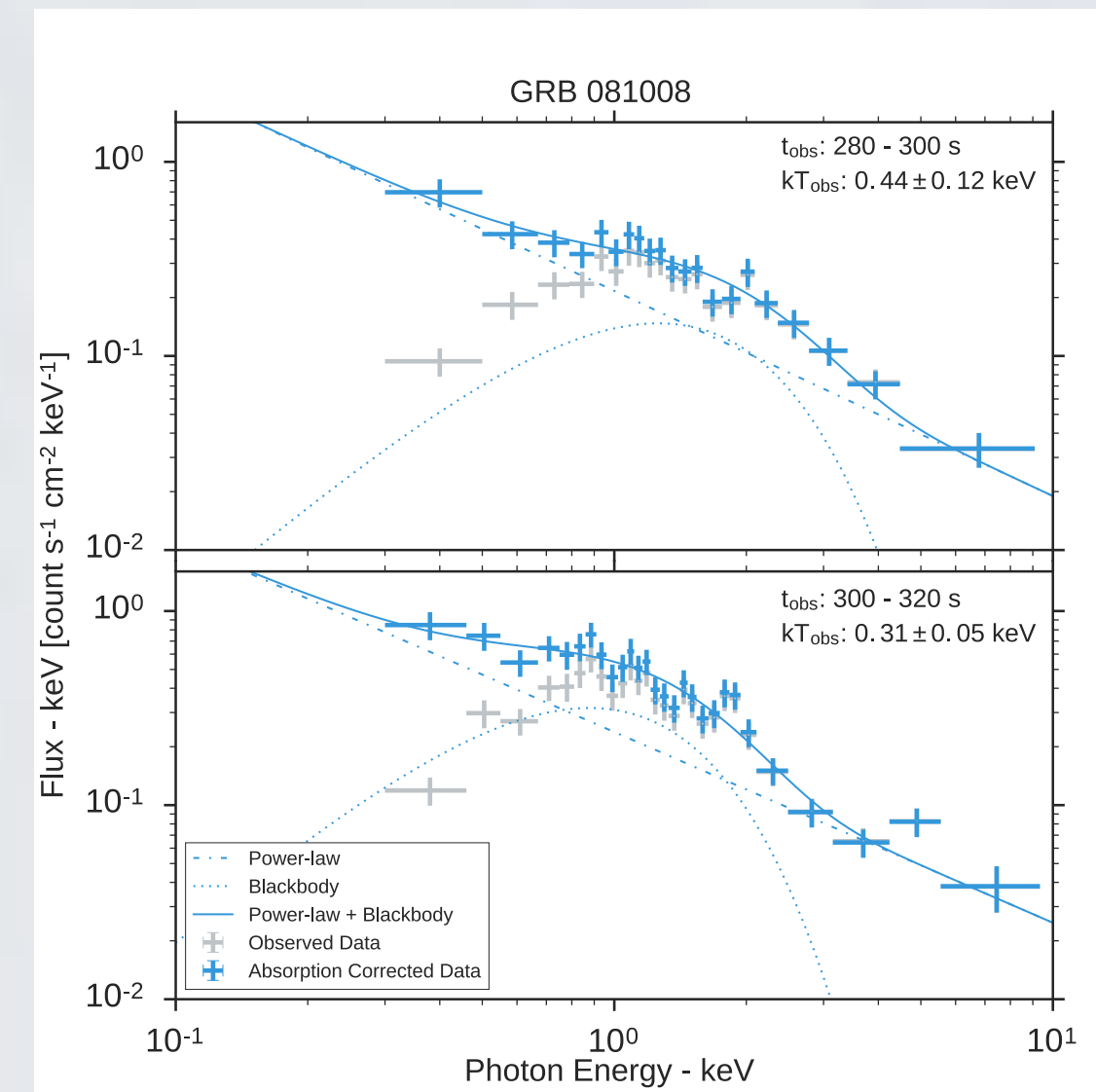
$$\beta = \Theta(\beta)^2 \frac{1 - \beta \cos \vartheta}{\sqrt{1 - \beta^2}} (1+z) \frac{\Delta R_{\text{nonrel}}}{c \Delta t_a^d}$$

THERMAL COMPONENT

Example

Example of GRB 081008, the thermal emitter expands mild-relativistically, at radius $\sim 10^{12}$ cm, and the temperature decays along the expansion.

Time interval	$280 \text{ s} \leq t_a^d \leq 300 \text{ s}$	$300 \text{ s} \leq t_a^d \leq 320 \text{ s}$
T_{obs} [keV]	0.44 ± 0.12	0.31 ± 0.05
R_{nonrel} [cm]	$(5.6 \pm 3.2) \times 10^{11}$	$(1.44 \pm 0.48) \times 10^{12}$
$\langle \beta \rangle_{(\cos \vartheta=1)}$	$0.90^{+0.06}_{-0.31}$	
$\langle \Gamma \rangle$		$2.34^{+1.29}_{-1.10}$
R_{lab} [cm]	$(7.1 \pm 4.1) \times 10^{11}$	$(2.34 \pm 0.78) \times 10^{12}$



Temperature and Radius

These blackbodies have fluxes in a range from 1% to 30% of the total flux and share similar order of magnitude radii.

In order to have a high significant thermal component, the blackbody radiation itself should be prominent, as well as its ratio to the non-thermal part. Another reason is that the observable temperature must be compatible with the satellite bandpass.

GRB	Radius (cm)	kT_{obs} (keV)	Significance
060204B	$1.80(\pm 1.11) \times 10^{11}$	$0.60(\pm 0.15)$	0.986
060607A	$1.67(\pm 1.01) \times 10^{11}$	$0.92(\pm 0.24)$	0.991
070318	<i>unconstrained</i>	$1.79(\pm 1.14)$	0.651
080607	$1.52(\pm 0.72) \times 10^{12}$	$0.49(\pm 0.10)$	0.998
080805	$1.12(\pm 1.34) \times 10^{11}$	$1.31(\pm 0.59)$	0.809
080810	$2.34(\pm 4.84) \times 10^{11}$	$0.61(\pm 0.57)$	0.999
081008	$1.84(\pm 0.68) \times 10^{12}$	$0.32(\pm 0.03)$	0.999
081210	<i>unconstrained</i>	$0.80(\pm 0.51)$	0.295
090516A	<i>unconstrained</i>	$1.30(\pm 1.30)$	0.663
090812	$1.66(\pm 1.84) \times 10^{12}$	$0.24(\pm 0.12)$	0.503
131030A	$3.67(\pm 1.02) \times 10^{12}$	$0.55(\pm 0.06)$	0.999
140206A	$9.02(\pm 2.84) \times 10^{11}$	$0.54(\pm 0.07)$	0.999
140301A	<i>unconstrained</i>	<i>unconstrained</i>	0.00
140419A	$1.85(\pm 1.17) \times 10^{12}$	$0.23(\pm 0.05)$	0.88
141221A	$1.34(\pm 2.82) \times 10^{12}$	$0.24(\pm 0.24)$	0.141
151027A	$1.18(\pm 0.67) \times 10^{12}$	$0.29(\pm 0.06)$	0.941

AT2019AT	$101 \times 10^{11} \times (79.0 \pm 81.1)$	$0.60(\pm 0.0)$	146.0
AT2019AT	$101 \times 10^{11} \times (28.2 \pm 42.1)$	$0.40(\pm 0.0)$	141.0
AT2019AT	$101 \times 10^{11} \times (11.1 \pm 28.1)$	$0.00(\pm 0.0)$	88.0

X-RAY FLARES

MODEL & SIMULATION

Modeling

We here examine the possibility that the flare originates from a fraction of the e^+e^- plasma interacting with the dense medium of the SN ejecta.

We start with the shape of the SN ejecta, following the results of the numerical simulations, then numerically solve the hydrodynamical equations.

$$\frac{\partial(\rho\Gamma)}{\partial t} + \nabla \cdot (\rho\Gamma\mathbf{v}) = 0$$

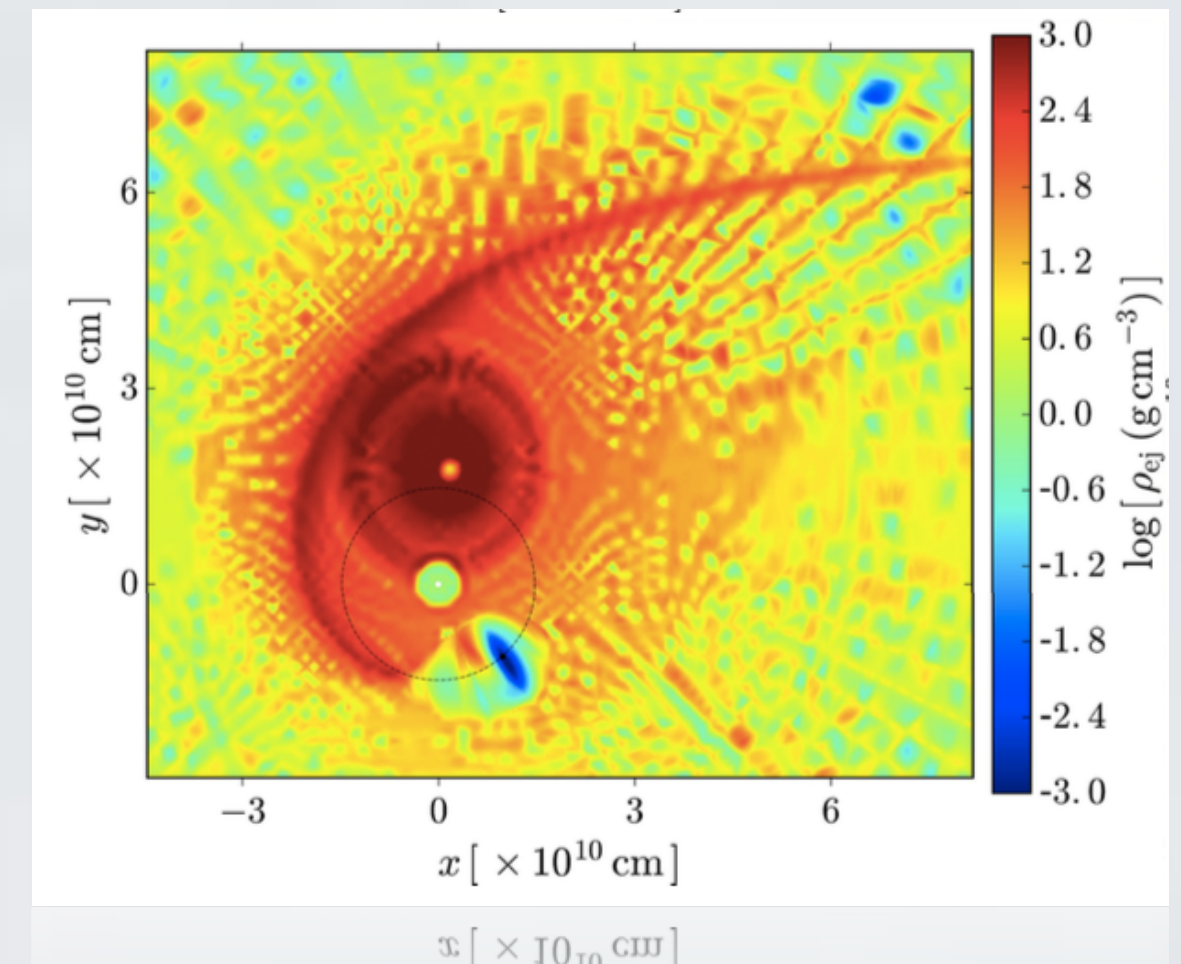
$$\frac{\partial m_r}{\partial t} + \nabla \cdot (m_r\mathbf{v}) + \frac{\partial p}{\partial r} = 0$$

$$\frac{\partial \mathcal{E}}{\partial t} + \nabla \cdot (\mathbf{m} - \rho\Gamma\mathbf{v}) = 0$$

Fluid momentum: $\mathbf{m} = h\Gamma^2\mathbf{v}$

Co-moving enthalpy: $h = \rho + \epsilon + p$

Internal energy density: $\mathcal{E} = h\Gamma^2 - p - \rho\Gamma$

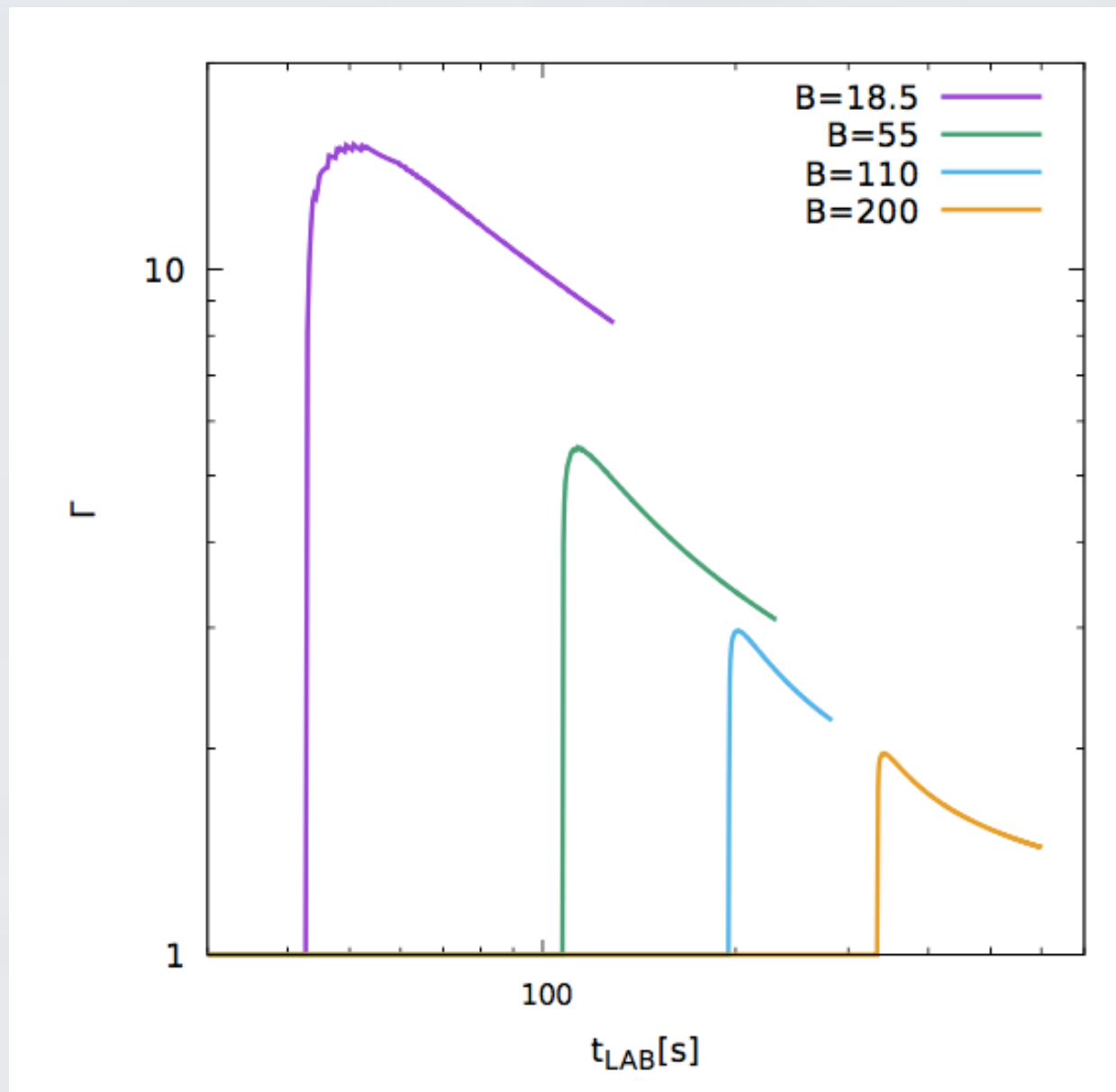


MODEL & SIMULATION

Simulation Result

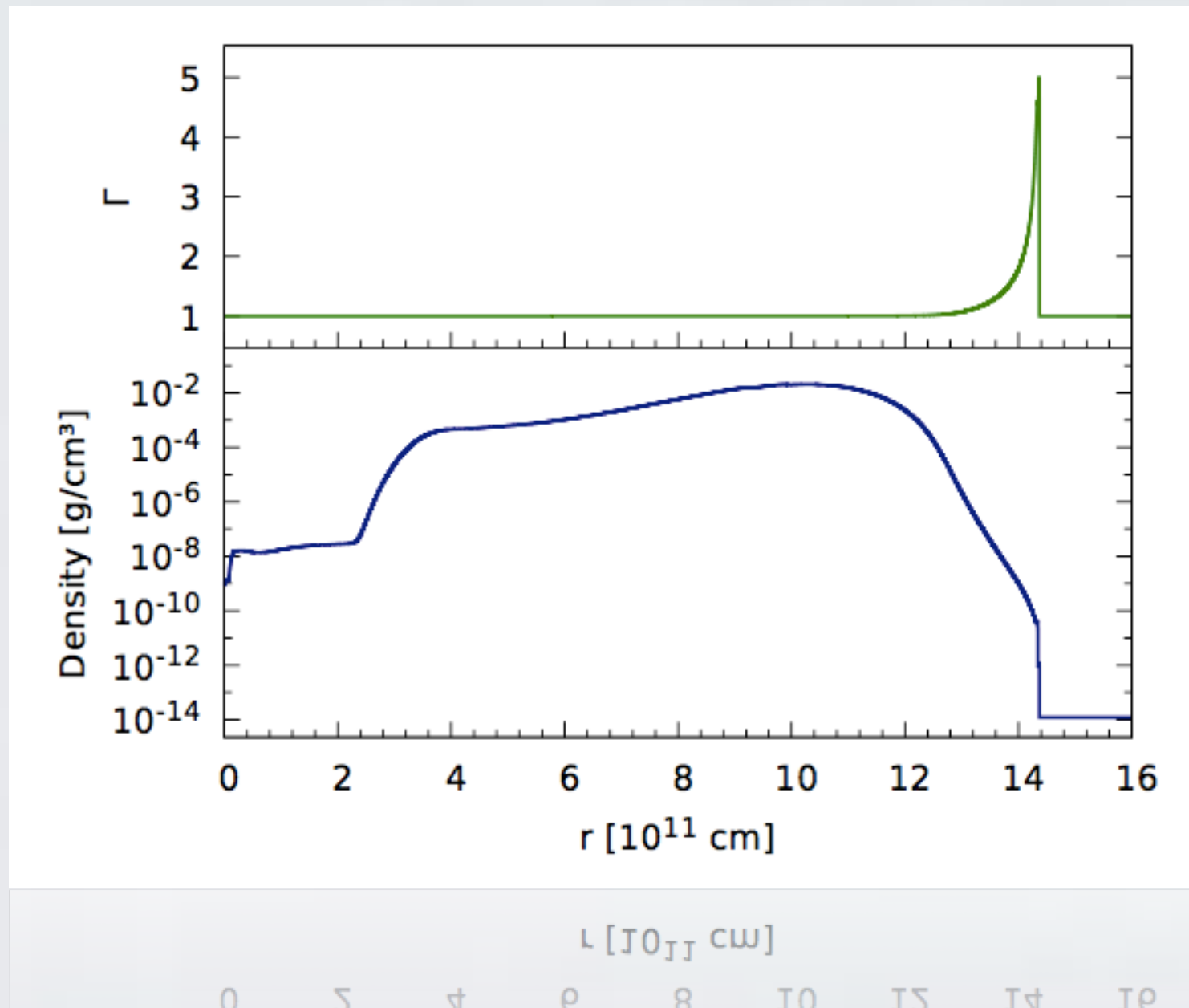
Lorentz factor of the emitting surface as a function of the laboratory time $E_{e^+e^-} = 3.16 \times 10^{53}$ erg and different selected values of the baryon load parameter $B = M_b c^2 / E_{e^+e^-}$.

Different B correspond to different directions inside the SN ejecta. We see that these results are in agreement with the Lorentz factor < 4 inferred from the thermal emission observed in the flare.



Simulation Result

Lorentz and mass density in the laboratory frame in the moment the plasma reaches the external surface of the SN ejecta. The profiles are made using a baryon load $B=200$. A shock is observed with a velocity distribution peaked at its exterior border. The maximum Lorentz factor at such a border is ~ 5 , while ~ 2 as can be seen at the transparent radius.



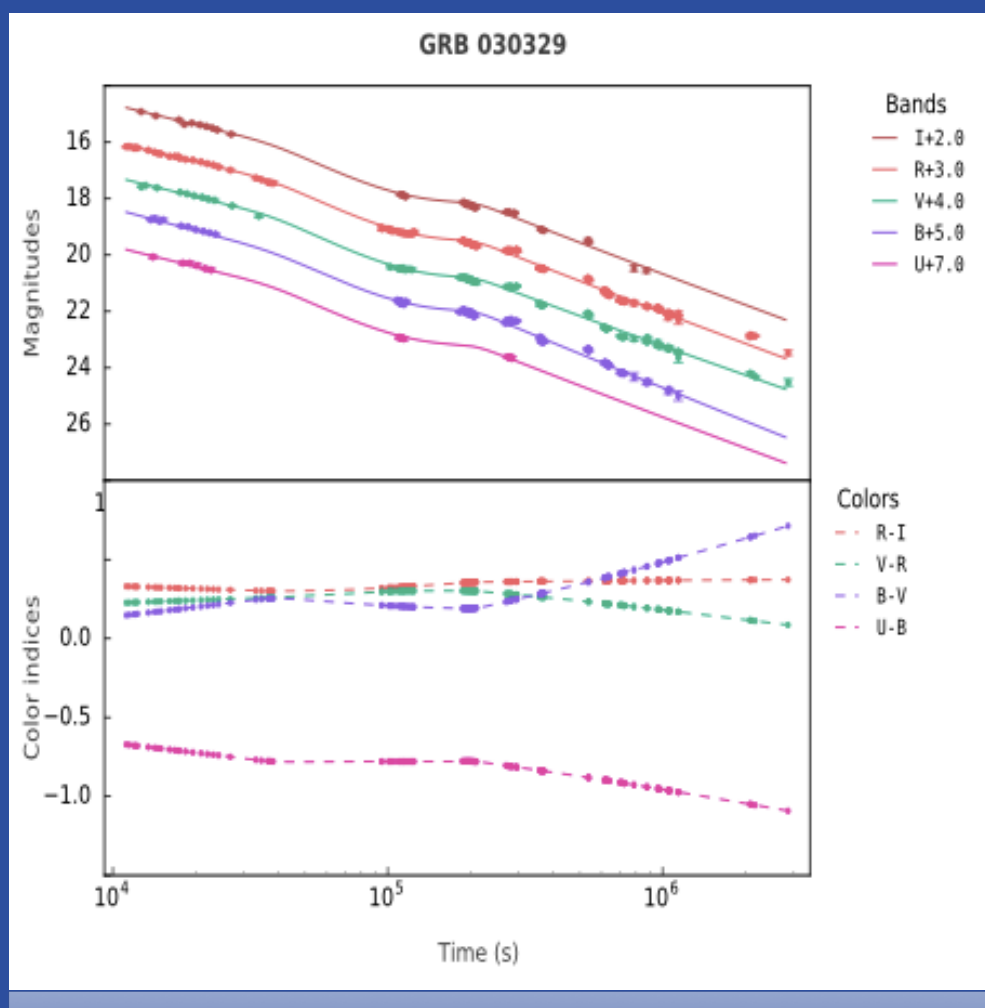
CONCLUSION

- Sample selection: 16 GRBs selected by criteria for having very clear flares form a possibly a same mechanism.
- Statistical Correlations between Eiso and flares features are found, which implies the association between X-ray flare and prompt emission.
- Thermal emission exists in the X-ray flares, and the thermal emitter expands mild-relativistically at radius $\sim 10^{12}$ cm.
- Modeling the flare generated by the collision of plasma outflow and the SN ejecta well fits the observation.

“Thank you”

A LARGE CATALOG OF MULTI-WAVELENGTH GRB AFTERGLOWS

- Colors Evolution And Their Physical Implication (Submitted)



Liang Li, Yu Wang, et al.,

